# Pyrene Synthesis in Circumstellar Envelopes and Its Role in the Formation of 2D Nanostructures

**Long Zhao, Ralf I. Kaiser***

*Department of Chemistry, University of Hawaii at Manoa, Honolulu, HI 96822, USA*

**Bo Xu, Utuq Ablikim, Musahid Ahmed**

*Chemical Sciences Division, Lawrence Berkeley National Laboratory, Berkeley, CA 94720, USA*

**Dharati Joshi, Gregory Veber, Felix R. Fischer**

*Department of Chemistry, University of California, Berkeley, CA 94720, USA*

*Materials Sciences Division, Lawrence Berkeley National Laboratory, Berkeley, CA 94720, USA*

*Kavli Energy Nano Sciences Institute at the University of California Berkeley and the Lawrence Berkeley National Laboratory, Berkeley, California 94720, USA*

**Alexander M. Mebel**

*Department of Chemistry and Biochemistry, Florida International University, Miami, FL 33193, USA*

**For the last decades, the Hydrogen-Abstraction/aCetylene-Addition (HACA) mechanism has been instrumental in attempting to untangle the origin of polycyclic aromatic hydrocarbons (PAHs) as identified in carbonaceous meteorites such as in Allende and Murchison. Notwithstanding, the fundamental reaction mechanisms leading to the synthesis of PAHs beyond phenanthrene ($C_{14}H_{10}$) are still unknown. By exploring the reaction of the 4-phenanthrenyl radical ($[C_{14}H_9]^{\bullet}$) with acetylene ($C_2H_2$) under conditions prevalent in carbon-rich circumstellar environments, we provide testimony on a facile, isomer-selective formation of pyrene ($C_{16}H_{10}$). Along with the Hydrogen Abstraction – Vinylacetylene Addition (HAVA) mechanism, molecular mass growth processes from pyrene may lead through systematic ring expansions not only to more complex PAHs, but ultimately to two-dimensional graphene-type structures. These fundamental reaction mechanisms are of crucial significance to facilitate an understanding of the origin and evolution of the molecular universe and in particular of carbon in our galaxy.**

## Introduction

The omnipresence of polycyclic aromatic hydrocarbons (PAHs) – organic molecules comprising fused benzene rings – along with alkylated (methyl, ethyl),[1] ionized, (de)hydrogenated, and protonated counterparts in the interstellar medium advocates that PAHs may comprise up to 20% of the carbon budget in our galaxy (Figure 1).[2-4] The pervasive existence of these molecules has been inferred from diffuse interstellar bands (DIBs)[5,6] – discrete absorption features superimposed on the interstellar extinction curve ranging from the blue part of the visible (400 nm) to the near-infrared (1.2 μm) – and from unidentified infrared (UIR) emission bands observed in the range of 3-14 μm[7]. The discovery of PAHs in carbonaceous chondrites such as in Allende and Murchison suggests a circumstellar origin.[8-11] Comprehensive $^{13}C/^{12}C$ and D/H isotopic analyses suggest that kinetically controlled molecular mass growth processes involve the synthesis of higher molecular weight PAHs from lower homologs[12-16] with prevailing astrochemical reaction models of PAH formation derived from those developed by the combustion community.[17-20]

The Hydrogen-Abstraction/aCetylene-Addition (HACA) mechanism has been exceptionally influential in attempting to unravel the synthesis of PAHs in outflows of carbon-rich asymptotic giant branch (AGB) stars.[21-23] Kinetic models[24-26] and electronic structure calculations[22,27-29] invoke HACA, which implicates a repetitive series of atomic hydrogen abstractions from the aromatic hydrocarbon trailed by consecutive addition of one or two acetylene molecule(s) prior to cyclization and aromatization.[21,22,26] Recently, Parker et al. demonstrated unequivocally that the simplest PAH comprised of two laterally fused benzene rings – the naphthalene molecule ($C_{10}H_8$) – can be formed via successive reactions of the phenyl radical with two acetylene molecules involving HACA.[18] Furthermore, phenanthrene ($C_{14}H_{10}$), which consists of three conjugated six-membered rings, was synthesized via reaction of the biphenylyl radical ($[C_{12}H_9]^{\bullet}$) with a single acetylene molecule through addition to the radical site followed by cyclization and aromatization.[20,30] However, the validity of HACA to form PAHs beyond phenanthrene has remained uncharted, since not a single experimental study could substantiate to what extent more complex PAHs beyond phenanthrene ($C_{14}H_{10}$) can be synthesized via molecular mass growth processes. Therefore, the omnipresence of PAHs in circumstellar and interstellar environments on one hand, but the hitherto elusive synthetic routes to complex PAHs on the other hand signifies a critical challenge in astrochemistry.

Here, by untangling the hitherto unknown chemistry of the 4-phenanthrenyl radical ($[C_{14}H_9]^{\bullet}$; 177 amu) with acetylene ($C_2H_2$; 26 amu) under conditions prevailing in circumstellar envelopes, we

unravel the previously elusive reaction mechanism leading to the synthesis of pyrene ($C_{16}H_{10}$; 202 amu) along with atomic hydrogen (1 amu) (reaction (1)). Our combined experimental and *ab initio* investigation revealed for the very first time the unambiguous formation of the prototype of a tetracyclic PAH carrying four fused benzene rings – pyrene – via molecular mass growth processes through the elementary reaction of an aromatic radical – 4-phenanthrenyl, which is formed via pyrolysis from a 4-bromophenanthrene precursor - with a single acetylene molecule involving a bay-closure mechanism. The pyrene molecule represents *the* key intermediate in mass growth processes of PAHs leading eventually to two dimensional carbonaceous nanostructures such as graphene. Likewise, pyrene represents *the* smallest PAH capable of forming relatively strongly bound dimers undergoing intermolecular coagulation.[31] This could result in the synthesis of three-dimensional structures like graphite thus bringing us closer to an understanding on the molecular carbon budget in our galaxy and the fundamental processes at molecular level synthesizing PAHs. The dimerization of PAH was believed to be a critical step in kinetic models for soot formation in combustion, which is required to reproduce correctly the soot particle size distribution. However, a combined experimental and theoretical study[32] on pyrene dimer demonstrated that carbon particle formation cannot rely upon physical dimerization of pyrene in hot environments at temperatures higher than 200 K. Therefore, chemical pathways are required for PAH growth and coagulation at high temperatures and those are proposed in the present work.

**Results – Laboratory Data**

Briefly, a high temperature chemical reactor was exploited to synthesize pyrene via the bimolecular reaction of the 4-phenanthrenyl radical with acetylene;[33,34] the isomer-specific products were probed by fragment-free photoionization of the products in a molecular beam by tunable vacuum ultraviolet (VUV) light in conjunction with the detection of the ionized molecules in a reflectron time-of-flight mass spectrometer (Re-TOF-MS) (Methods). A representative mass spectrum recorded at a photoionization energy of 9.50 eV for the reaction the 4-phenanthrenyl radical with acetylene is displayed in Figure 2a; reference spectra were also collected by substitu-

(1) $$[C_{14}H_9]^{\bullet} + C_2H_2 \rightarrow C_{16}H_{10} + H^{\bullet}$$

ting the acetylene reactant with the non-reactive helium carrier gas (Figure 2b). These data provide compelling proof on the synthesis of a molecule with the molecular formula $C_{16}H_{10}$ (202 amu) in the 4-phenanthrenyl/acetylene system (Figure 2a), which is lacking in the control experiment (Figure 2b). Accounting for the molecular weight of the reactants and the products, we deduce that

the $C_{16}H_{10}$ molecule(s) along with atomic hydrogen is synthesized via the reaction (1) of 4-phenanthrenyl with acetylene. Signals at mass-to-charge ratios (*m/z*) of 259 ($C_{13}{}^{13}CH_9{}^{81}Br^+$), 258 ($C_{14}H_9{}^{81}Br^+$), 257($C_{13}{}^{13}CH_9{}^{79}Br^+$), 256 ($C_{14}H_9{}^{79}Br^+$), 179 ($C_{13}{}^{13}CH_{10}{}^+$), 178 ($C_{14}H_{10}{}^+$), 177($C_{14}H_9{}^+/C_{14}{}^{13}CH_8{}^+$), and 176($C_{14}H_8{}^+$) are observable in both the 4-phenanthrenyl/ acetylene and the 4-phenanthrenyl/helium systems – albeit at different ratios. Hence, these masses do not originate from reactions between 4-phenanthrenyl and acetylene. Signal at *m/z* = 259 to 256 can be associated with the non-pyrolyzed 4-bromophenanthrene precursor; signal at *m/z* = 178 and 179 is attributed to phenanthrene and $^{13}$C-phenanthrene formed via hydrogen addition to the 4-phenanthrenyl radical; finally, ion counts at *m/z* = 176 and 177 are linked to phenanthryne isomers (*m/z* = 176) along with the 4-phenanthrenyl radical ($[C_{14}H_9]^{\bullet+}$; *m/z* = 177) (Supplementary Information). It is important to note that under our experimental conditions, the injection of pure acetylene ($C_2H_2$) into our reactor does not lead to the formation of any PAHs.[18]

Considering the discovery of hydrocarbon molecule(s) with the molecular formula $C_{16}H_{10}$ formed in the reaction of 4-phenanthrenyl with acetylene, it is our goal to identify the structural isomer(s) formed. This warrants a detailed analysis of the corresponding photoionization efficiency (PIE) curve, which depicts the intensity of the ions at *m/z* of 202 ($C_{16}H_{10}{}^+$) as a function of the photon energy from 7.30 eV to 10.00 eV (Figure 3a). This function is matched with known reference PIE curves for distinct $C_{16}H_{10}$ isomers. The experimentally derived PIE curve at *m/z* of 202 (black) can be reproduced effectively by a linear combination of two reference PIE curve of pyrene ($C_{16}H_{10}{}^+$; green) and of ethynylphenanthrenes ($C_{16}H_{10}{}^+$; blue) with the overall fit superimposed in red. The experimental and reference PIE curves for pyrene illustrate both onsets of the ion signal at 7.40 ± 0.05 eV; this onset correlates nicely with the adiabatic ionization energy of pyrene of 7.426 ± 0.001 eV.[35] The PIE curves and adiabatic ionization energies of distinct isomers of ethynylphenanthrenes of 7.72 ± 0.10 eV are quite similar within our error limits (Supplementary Information), and we cannot determine explicitly which ethynylphenanthrene isomer(s) is(are) formed; however, since our reaction was carried out with 4-phenanthrenyl, we may expect the formation of 4-ethynylphenanthrene. The outcome of comparable PIE curves of ethynyl-substituted aromatic compounds for the phenanthrene system mirrors closely our findings for ethynyl-substituted naphthalene isomers.[19] It should be stressed that the PIE curve for *m/z* = 203 (Figure 3b) is, after scaling, superimposable on the PIE curve of *m/z* = 202; further, the PIE curve of *m/z* = 203 can be also fit with a linear combination of pyrene and ethynylphenanthrenes. Consequently, the PIE graph of *m/z* = 203 can be attributed to $^{13}$C substituted isomers ($C_{15}{}^{13}CH_{10}$) of pyrene and

ethynylphenanthrenes ($C_{16}H_{10}$). It is important to highlight that the PIE curves of $C_{16}H_{10}$ isomers of pyrene and ethynylphenanthrenes are *characteristically correlated* to each molecule stressing that the co-existence of alternative isomers in the molecular beam would change the shape of the PIE significantly. Therefore, we conclude that pyrene and ethynylphenanthrenes represent the only contributors to signal at *m/z* of 202 and 203 within our error limits. Two sources contribute to the errors, i.e. ± 10% based on the accuracy of the photodiode and a 1 σ error of the PIE curve averaged over three scans.

**Results – Computational Data**

Our study reveals for the very first time that the prototype of a PAH composed of four fused benzene rings – pyrene – can be formed via the bimolecular reaction of the 4-phenanthrenyl radical with acetylene at elevated temperatures of 1400 K. Augmented by electronic structure calculations of the pertinent $C_{16}H_{10}$ and $C_{16}H_{11}$ potential energy surfaces (PESs) (Figure 4) (Methods), this reaction is initiated by the addition of the radical center of 4-phenanthrenyl to the acetylene molecule through an entrance barrier of 20 kJ mol$^{-1}$ leading to the intermediate **[i1]** followed by ring-closure of the $C_{16}H_{11}$ collision complex via a transition state located 26 kJ mol$^{-1}$ above the complex leading to **[i2]**. This entrance barrier can be easily overcome in high temperature circumstellar environments holding temperatures of a few 1000 K. The tetracyclic $[C_{16}H_{11}]^{\bullet}$ intermediate **[i2]** ultimately undergoes unimolecular decomposition via atomic hydrogen elimination and aromatizes via a tight transition state located 41 kJ mol$^{-1}$ above the energy of the separated products forming pyrene (**p1**) plus atomic hydrogen in an overall exoergic reaction (–246 kJ mol$^{-1}$). Alternative reaction pathways to pyrene (**p1**) were located as well. However, considering the inherent barrier of the hydrogen shift from **[i2]** to **[i5]** followed by atomic hydrogen loss to pyrene (**p1**) compared to the energetics of the exit transition state for the unimolecular decomposition of [**i2**], the **[i2]** → **[i5]** → **p1** + H$^{\bullet}$ route is less competitive. Alternatively, according to the calculated rate constants for the **[i1]** → **[i3]** and **[i1]** → **[i4]** reactions in our work, the pathway involving the hydrogen migration from **[i1]** to **[i4]** followed by ring closure to **[i5]** and then hydrogen loss provides a comparable contribution to the formation of pyrene and becomes slightly preferable compared to the **[i2]** → **[i5]** → **p1** plus hydrogen channel at temperatures above 1375 K. A question arises on the formation of alternative $C_{16}H_{10}$ isomers such as the 4-ethynylphenenthrene molecule (**p2**). A close look at the pertinent section of the PES reveals that **[i1]** either emits a hydrogen atom to form **p2** or undergoes a hydrogen shift from the acetylenic moiety to the phenanthrene ring

yielding **[i3]** prior to hydrogen loss forming 4-ethynylphenenthrene in an overall slightly exoergic reaction (–17 kJ $mol^{-1}$). Since the energies of the critical transition states for these two channels are relatively close, both channels provide contributions to the formation of ethynylphenanthrene but that of the two-step pathway decreases with temperature due to the higher entropy demands.

Having elucidated the synthesis of pyrene via the reaction of the 4-phenanthrenyl radical with acetylene, we are conveying these findings now to the 'real' circumstellar environments. Here, our statistical (RRKM-Master Equation) calculations deliver critical temperature-dependent rate constants for the 4-phenanthrenyl plus acetylene reaction at nearly zero pressure conditions prevailing in circumstellar envelopes of carbon stars. Supplementary Figure 3 illustrates the calculated rate constants at the zero- and high-pressure limits. The dependence of the rate constants on pressure is rather weak, slight difference between zero and high pressure is seen only at high temperatures above 1800 K and the maximal deviation is observed at 4000 K, where the total rate constant at zero pressure is a factor of about two lower than the high-pressure limit value. The reaction is dominated by the formation of pyrene up to 3000 K. The branching ratio of ethynylphenanthrene gradually increases with temperature, from a few per cent at 1400–1500 K to 11%, 51%, and 79% at 2000 K, 3000 K, and 4000 K, respectively. The calculated rate constant for the formation of pyrene remains high, $1–3 \times 10^{-12}$ $cm^3$ $molecule^{-1}$ $s^{-1}$, at temperatures above 1500 K.

## Astrophysical Implications

The synthetic pathway to pyrene defines a prototype pattern of a HACA-type bay closure on an armchair edge of a PAH molecule. In circumstellar envelopes of dying carbon stars, the 4-phenanthrenyl/acetylene route might be triggered by the abstraction of a hydrogen atom from the 4-carbon position of a phenanthrene molecule ($C_{14}H_{10}$), which in turn can be synthesized via the elementary reaction of the *o*-biphenylyl radical ($[C_6H_5–C_6H_4]^•$) with a single acetylene molecule (Figure 5);[20] the *o*-biphenylyl radical is formed through hydrogen abstraction from biphenyl ($C_6H_5–C_6H_5$), which itself is generated via the bimolecular reaction of the phenyl radical ($[C_6H_5]^•$) with benzene ($C_6H_6$).[36] Therefore, HACA-type pathways to pyrene ($C_{16}H_{10}$) commence with the biphenyl molecule and involve two successive hydrogen abstraction/acetylene addition sequences, but not with the naphthyl radical ($[C_{10}H_7]^•$) as postulated previously in astrophysical models.

However, solely HACA-type pathways cannot account for more complex PAHs such as benzo[*e*]pyrene (Figure 1). Upon hydrogen abstraction from pyrene ($C_{16}H_{10}$), the pyrenyl radical ($C_{16}H_9^•$) would add an acetylene molecule ($C_2H_2$) yielding a $C_{18}H_{11}$ radical intermediate (Figure 5).

As demonstrated in electronic structure calculations[29,37] and verified experimentally for the naphthyl/acetylene system,[19] the $C_{18}H_{11}$ radical is expected to undergo cyclization followed by atomic hydrogen loss to cyclopenta[*cd*]pyrene ($C_{18}H_{10}$) rather than adding a second acetylene molecule succeeded by cyclization and hydrogen loss to benzo[*e*]pyrene ($C_{20}H_{12}$). Therefore, alternative reaction mechanisms to HACA such as the recently exposed hydrogen abstraction/ vinylacetylene addition (HAVA) mechanism[17] must be involved in the formation of more complex PAHs such as benzo[*e*]pyrene and even dibenzo[*h,rst*]pentaphene (Figure 5). HAVA represents a barrier-less reaction pathway and leads to PAH growth via six-membered ring-expansions via a single collision event. This finding also supports Harada et al.'s conclusion based on a detailed $^{13}C/^{12}C$ isotopic analysis identifying pyrene as a central PAH intermediate leading to a two-dimensional network of PAHs consisting solely of fused benzene rings up to benzo[*ghi*]-perylene.[14] The complementary nature of the HACA and HAVA mechanisms and their role in the build-up of two-dimensional graphene-type nanostructures is best visualized in Supplementary Figure 4. Starting from pyrene, the vinylacetylene (HAVA) route leads to a radial acene-type growth in three segments of the plane separated by 120°, whereas acetylene (HACA) accounts for the bay closure. Once HACA closes all bays, HAVA initiates a third order perimeter growth (Supplementary Figure 4(g)) generating new bays to be closed. This pathway may ultimately lead to graphene-like nanostructures and – after condensation of multiple layers – to graphitized carbon with grain sizes of up to 80 nm as detected in carbonaceous chondrites like Allende and Murchison.[8,38-42]

## Conclusions

In summary, the facile route to pyrene ($C_{16}H_{10}$) as detected in carbonaceous chondrites via the elementary reaction of the 4-phenanthrenyl radical with acetylene leads to the synthesis of a key building block in the successive growth of two-dimensional (graphene-type) nanostructures. The molecular growth processes has to involve highly complementary HAVA and HACA routes leading to a radial PAH expansion through acene-like structures and bay-closures, respectively (Figure 5), but cannot proceed via simple pyrene dimerization at temperatures above 200 K as demonstrated by Sabbah et al.[32] The incorporation of five-membered rings formed through the reaction of pyrene ($C_{16}H_{10}$) with acetylene ($C_2H_2$) via HACA, on the other hand, may form acenaphthylene-like building blocks (Figure 5); successive HACA and HAVA sequences may potentially synthesize non-planar PAHs holding corannulene units and three-dimensional carbonaceous nanostructures proposed to exist in chondrites[43,44] and fullerenes as detected in the planetary nebulae TC 1.[45] We

would like to point out that PAHs formed in outflows of AGB stars can be degraded by the harsh environment of the ISM (photons, shocks, galactic cosmic rays) and by processing in the protoplanetary disk[3,15,46-48] with Micelotta et al. predicting PAH lifetimes against these destruction processes of about $10^8$ years. However, the abundances of PAHs in meteorites are measured in ppm,[8,10] and the total PAH abundance injected by AGBs is in the order of 10% of the elemental carbon.[49,50] So it is clear from these data that the absolute fraction of PAHs formed in outflows of AGB stars and incorporated eventually in meteorites is small, but detectable serving as molecular tracers to allow astrochemists to deliver a rigorous experimentally verified mechanistic framework to explain the presence of PAHs in our galaxy. This will ultimately transform how we think about the origin and evolution of carbonaceous matter in the universe.

**References**

1 Elsila, J. E., de Leon, N. P., Buseck, P. R. & Zare, R. N. Alkylation of polycyclic aromatic hydrocarbons in carbonaceous chondrites. *Geochim. Cosmochim. Acta* **69,** 1349-1357 (2005).

2 D'Hendecourt, L. & Ehrenfreund, P. Spectroscopic properties of polycyclic aromatic hydrocarbons (PAHs) and astrophysical implications. *Adv. Space Res.* **19,** 1023-1032 (1997).

3 A. G. G. M. Tielens, C. Kerckhoven & E. Peeters, S. H. Astrochemistry: From molecular clouds to planetary systems. *Proceedings of IAU Symposium* **197,** 349-362 (2000).

4 Rhee, Y. M., Lee, T. J., Gudipati, M. S., Allamandola, L. J. & Head-Gordon, M. Charged polycyclic aromatic hydrocarbon clusters and the galactic extended red emission. *PNAS* **104,** 5274-5278 (2007).

5 Salama, F., Galazutdinov, G. A., Krelowski, J., Allamandola, L. J. & Musaev, F. A. Polycyclic aromatic hydrocarbons and the diffuse interstellar bands. A survey. *Astrophys. J.* **526,** 265-273 (1999).

6 Duley, W. W. Polycyclic aromatic hydrocarbons, carbon nanoparticles and the diffuse interstellar bands. *Faraday Discuss.* **133,** 415-425 (2006).

7 Ricks, A. M., Douberly, G. E. & Duncan, M. A. The infrared spectrum of protonated naphthalene and its relevance for the unidentified infrared bands. *Astrophys. J.* **702,** 301-306 (2009).

8 Messenger, S. *et al.* Indigenous polycyclic aromatic hydrocarbons in circumstellar graphite grains from primitive meteorites. *Astrophys. J.* **502,** 284-295 (1998).

9 Hahn, J. H., Zenobi, R., Bada, J. L. & Zare, R. N. Application of two-step laser mass spectrometry to cosmogeochemistry: Direct analysis of meteorites. *Science* **239,** 1523-1525 (1988).

10 Zenobi, R., Philippoz, J.-M., Buseck, P. R. & Zare, R. N. Spatially resolved organic analysis of the allende meteorite. *Science* **246,** 1026-1029 (1989).

11 Plows, F. L., Elsila, J. E., Zare, R. N. & Buseck, P. R. Evidence that polycyclic aromatic hydrocarbons in two carbonaceous chondrites predate parent-body formation. *Geochim. Cosmochim. Acta* **67,** 1429-1436 (2003).

12 Gilmour, I. & Pillinger, C. T. Isotopic compositions of individual polycyclic aromatic hydrocarbons from the murchison meteorite. *Mon. Not. Royal Astron. Soc.* **269,** 235-240 (1994).

13 Naraoka, H., Shimoyama, A. & Harada, K. Molecular and isotopic distributions of pahs from three antarctic carbonaceous chondrites (CM2). *Mineral. Mag.* **62A,** 1056-1057 (1998).

14 Naraoka, H., Shimoyama, A. & Harada, K. Isotopic evidence from an antarctic carbonaceous chondrite for two reaction pathways of extraterrestrial PAH formation. *Earth Planet. Sci. Lett.* **184,** 1-7 (2000).

15 Tielens, A. G. G. M. Interstellar polycyclic aromatic hydrocarbon molecules. *Annu. Rev. Astron. Astr.* **46,** 289-337 (2008).

16 Tielens, A. G. G. M. The molecular universe. *Rev. Mod. Phys.* **85,** 1021-1081 (2013).

17 Parker, D. S. *et al.* Low temperature formation of naphthalene and its role in the synthesis of pahs (polycyclic aromatic hydrocarbons) in the interstellar medium. *PNAS* **109,** 53-58 (2012).

18 Parker, D. S., Kaiser, R. I., Troy, T. P. & Ahmed, M. Hydrogen abstraction/acetylene addition revealed. *Angew. Chem.-Int. Edit.* **53,** 7740-7744 (2014).

19 Parker, D. S. N. *et al.* Unexpected chemistry from the reaction of naphthyl and acetylene at combustion-like temperatures. *Angew. Chem.-Int. Edit.* **54,** 5421-5424 (2015).

20 Yang, T. *et al.* HACA's heritage: A free-radical pathway to phenanthrene in circumstellar envelopes of asymptotic giant branch stars. *Angew. Chem.-Int. Edit.* **56,** 4515-4519 (2017).

21 Frenklach, M. & Feigelson, E. D. Formation of polycyclic aromatic hydrocarbons in circumstellar envelopes. *Astrophys. J* **341,** 372-384 (1989).

22 Richter, H. & Howard, J. B. Formation of polycyclic aromatic hydrocarbons and their growth to soot - a review of chemical reaction pathways. *Prog. Energy Combust. Sci.* **26,** 565-608 (2000).
23 Frenklach, M. Reaction mechanism of soot formation in flames. *Phys. Chem. Chem. Phys.* **4,** 2028-2037 (2002).
24 Frenklach, M., Clary, D. W., Gardiner, W. C. & Stein, S. E. Detailed kinetic modeling of soot formation in shock-tube pyrolysis of acetylene. *Proc. Combust. Inst.* **20,** 887-901 (1985).
25 Wang, H. & Frenklach, M. Calculations of rate coefficients for the chemically activated reactions of acetylene with vinylic and aromatic radicals. *J. Phys. Chem.* **98,** 11465-11489 (1994).
26 Appel, J., Bockhorn, H. & Frenklach, M. Kinetic modeling of soot formation with detailed chemistry and physics: Laminar premixed flames of C2 hydrocarbons. *Combust. Flame* **121,** 122-136 (2000).
27 Marsh, N. D. & Wornat, M. J. Formation pathways of ethynyl-substituted and cyclopentafused polycyclic aromatic hydrocarbons. *Proc. Combust. Inst.* **28,** 2585-2592 (2000).
28 Tokmakov, I. V. & Lin, M. C. Reaction of phenyl radicals with acetylene: Quantum chemical investigation of the mechanism and master equation analysis of the kinetics. *J. Am. Chem. Soc.* **125,** 11397-11408 (2003).
29 Kislov, V. V., Sadovnikov, A. I. & Mebel, A. M. Formation mechanism of polycyclic aromatic hydrocarbons beyond the second aromatic ring. *J. Phys. Chem. A* **117,** 4794-4816 (2013).
30 Chmielewski, A. G. *et al.* $NO_x$ and PAHs removal from industrial flue gas by using electron beam technology with alcohol addition. *Radiat. Phys. Chem.* **67,** 555-560 (2003).
31 Schuetz, C. A. & Frenklach, M. Nucleation of soot: Molecular dynamics simulations of pyrene dimerization. *Proc. Combust. Inst.* **29,** 2307-2314 (2002).
32 Sabbah, H., Biennier, L., Klippenstein, S. J., Sims, I. R. & Rowe, B. R. Exploring the role of PAHs in the formation of soot: Pyrene dimerization. *J. Phys. Chem. Lett.* **1,** 2962-2967 (2010).
33 Chen, P., Colson, S. D., Chupka, W. A. & Berson, J. A. Flash pyrolytic production of rotationally cold free radicals in a supersonic jet. Resonant multiphoton spectrum of the $3p^2A_2'' \leftarrow X^2A_2''$ origin band of methyl. *J. Phys. Chem.* **90,** 2319-2321 (1986).
34 Chen, P., Pallix, J. B., Chupka, W. A. & Colson, S. D. Resonant multiphoton ionization spectrum and electronic structure of CH radical. New states and assignments above 50,000 $cm^{-1}$. *J. Chem. Phys.* **86,** 516-520 (1987).
35 Photonionization Cross Section Database (Version 2.0), National Synchrotron Radiation Laboratory, Hefei, China. http://flame.nsrl.ustc.edu.cn/database/ (2017).
36 Zhang, F., Gu, X. & Kaiser, R. I. Formation of the diphenyl molecule in the crossed beam reaction of phenyl radicals with benzene. *J. Chem. Phys.* **128,** 084315 (2008).
37 Mebel, A. M., Landera, A. & Kaiser, R. I. Formation mechanisms of naphthalene and indene: From the interstellar medium to combustion flames. *J. Phys. Chem. A* **121,** 901-926 (2017).
38 Mostefaoui, S., Hoppe, P. & El Goresy, A. In situ discovery of graphite with interstellar isotopic signatures in a chondrule-free clast in an L3 chondrite. *Science* **280,** 1418-1420 (1998).
39 Smith, P. P. K. & Buseck, P. R. Carbon in the allende meteorite: Evidence for poorly graphitized carbon rather than carbyne. *Geochim. Cosmochim. Acta, Suppl.* **16,** 1167-1175 (1982).
40 Duley, W. W. Chemical evolution of carbonaceous material in interstellar clouds. *Astrophys. J.* **528,** 841-848 (2000).
41 Amari, S., Lewis, R. S. & Anders, E. Interstellar grains in meteorites: III. Graphite and its noble gases. *Geochim. Cosmochim. Acta* **59,** 1411-1426 (1995).

42 Zinner, E., Amari, S., Wopenka, B. & Lewis, R. S. Interstellar graphite in meteorites: Isotopic compositions and structural properties of single graphite grains from murchison. *Meteoritics* **30,** 209-226 (1995).
43 Garvie, L. A. J. & Buseck, P. R. Nanosized carbon-rich grains in carbonaceous chondrite meteorites. *Earth Planet. Sci. Lett.* **224,** 431-439 (2004).
44 Zega, T. J., Garvie, L. A. J., Dodony, I. & Buseck, P. R. Serpentine nanotubes in the Mighei CM chondrite. *Earth Planet. Sci. Lett.* **223,** 141-146 (2004).
45 Cami, J., Bernard-Salas, J., Peeters, E. & Malek, S. E. Detection of C60 and C70 in a young planetary nebula. *Science* **329,** 1180-1182 (2010).
46 Cherchneff, I., Barker, J. R. & Tielens, A. G. G. M. Polycyclic aromatic hydrocarbon formation in carbon-rich stellar envelopes. *Astrophys. J.* **401,** 269-287 (1992).
47 Cohen, M., Tielens, A. G. G. M. & Bregman, J. D. Mid-infrared spectra of WC 9 Stars: The composition of circumstellar and interstellar dust. *Astrophys. J.* **344,** L13-L16 (1989).
48 Micelotta, E., Jones, A. & Tielens, A. Polycyclic aromatic hydrocarbon processing in interstellar shocks. *A & A* **510,** A36 (2010).
49 Allamandola, L. J., Tielens, A. G. G. M. & Barker, J. R. Interstellar polycyclic aromatic hydrocarbons: The infrared emission bands, the excitation/emission mechanism, and the astrophysical implications. *Astrophys. J., Suppl. Ser.* **71,** 733-775 (1989).
50 Bernstein, M. P. *et al.* UV irradiation of polycyclic aromatic hydrocarbons in ices: Production of alcohols, quinones, and ethers. *science* **283,** 1135-1138 (1999).

**Corresponding Author**

RIK (ralfk@hawaii.edu)

**Acknowledgments**

This work was supported by the US Department of Energy, Basic Energy Sciences DE-FG02-03ER15411 (experimental studies), DE-FG02-04ER15570 (computational studies), and DE-SC0010409 (synthesis of precursor molecules) to the University of Hawaii, to Florida International University, and the University of California Berkeley, respectively. B.X., U.A., and M.A. along with the Advanced Light Source are supported by the Director, Office of Science, Office of Basic Energy Sciences, of the U.S. Department of Energy under Contract No. DE-AC02-05CH11231, through the Chemical Sciences Division. D.J. acknowledges support through a National Science Foundation Graduate Research Fellowship under Grant # DGE-1106400. The authors also thank Prof. Xander Tielens (University of Leiden, The Netherlands) for helpful discussions.

**Author contributions**

D.J. and G.V. synthesized the molecular precursor; L.Z., B.X., and U.A. carried out the experimental measurements; L.Z. performed the data analysis; A.M.M. carried out the theoretical analysis; R.I.K., A.M.M., and M.A. discussed the data; F.R.F. supervised the synthesis of the molecular precursor; R.I.K. designed the experiments and wrote the manuscript.

**Main Figure Legends**

Figure 1: Possible structures of isomers of aromatic molecules detected in carbonaceous meteorites. [1] biphenyl, [2] naphthalene, [3] anthracene, [4] phenanthrene, [5] triphenylene, [6] pyrene, [7] chrysene, [8] benz[*a*]anthracene, [9] benzo[*a*]pyrene, [10] benzo[*e*]pyrene.

Figure 2: Comparison of photoionization mass spectra recorded at a photoionization energy of 9.50 eV for the (a) 4-phenanthrenyl ($C_{14}H_9$)/acetylene ($C_2H_2$) and (b) 4-phenanthrenyl ($C_{14}H_9$)/helium systems. The mass peak of the $C_{16}H_{10}$ isomer(s) (*m/z* = 202) along with the $^{13}C$ substituted species (*m/z* = 203) are highlighted in red.

Figure 3: Photoionization efficiency (PIE) curves for *m/z* = 202 and 203. Black: experimentally derived PIE curves with the grey area defining the error. The red curve represents the overall fit based on a linear combination of the PIE reference curves of pyrene (green) and ethynylphenanthrene (blue). ± 10% uncertainty based on the accuracy of the photodiode and a 1 σ error of the PIE curve averaged over three PIE scans contribute to the overall errors.

Figure 4: Potential energy surface (PES) for the 4-phenanthrenyl $[C_{14}H_9]^{\bullet}$ reaction with acetylene ($C_2H_2$) calculated at the G3(MP2,CC)//B3LYP/6-311G(d,p) level of theory. The favorable pathways leading to pyrene are colored in red. The relative energies are given in kJ $mol^{-1}$.

Figure 5: Molecular mass growth processes to PAHs involving HACA and HAVA. Top: Reaction pathways involved in the synthesis of pyrene via HACA. Bottom: Reactions of the pyrenyl radical via HACA (red) and HAVA (blue); only the HAVA mechanism leads to expansion of the PAH structure by a six-membered ring to form benzo[*e*]pyrene and more complex PAHs carrying solely six-membered rings such as dibenzo[*h,rst*]pentaphene.

## Methods

**Experimental**: The experiments were carried out at the Chemical Dynamics Beamline (9.0.2) of the Advanced Light Source utilizing a resistively-heated silicon-carbide (SiC) chemical reactor interfaced to a molecular beam apparatus operated with a reflectron time-of-flight mass spectrometer (Wiley-McLaren Re-TOF-MS). The chemical reactor mimics the high temperature conditions together with discrete chemical reactions to form PAHs *in situ* through the reaction of radicals. Here, 4-phenanthrenyl radicals [$C_{14}H_9$]$^{\bullet}$ were prepared at concentrations of less than 0.1% *in situ* via pyrolysis of the 4-bromophenanthrene precursor ($C_{14}H_9Br$; Supplementary Information) seeded in acetylene carrier gas (0.394 ± 0.005 atm; $C_2H_2$; Matheson Gas). The acetylene gas acted as a carrier gas and as a reactant with the pyrolytically generated radicals. The temperature of the SiC tube was monitored using a Type-C thermocouple and was maintained at 1400 ± 10 K. The reaction products formed in the reactor were expanded supersonically and passed through a 2 mm diameter skimmer located 10 mm downstream the pyrolytic reactor and enter into the main chamber, which houses the Re-TOF-MS. The quasi-continuous tunable vacuum ultraviolet (VUV) light from the Advanced Light Source intercepted the neutral molecular beam perpendicularly in the extraction region of a Wiley-McLaren Re-TOF-MS. VUV single photon ionization signifies essentially a fragment-free ionization technique and hence is characterized as a *soft ionization* method compared to electron impact ionization, which the latter often leading to excessive fragmentation of the parent ion.[51-53] The ions formed via photoionization are extracted and fed onto a microchannel plate detector through an ion lens. Photoionization efficiency (PIE) curves, which report ion counts as a function of photon energy from 7.30 eV to 10.00 eV with a step interval of 0.05 eV at a well-defined mass-to-charge ratio (*m/z*), were produced by integrating the signal recorded at the specific *m/z* for the species of interest. Reference (blank) experiments were also conducted by expanding neat acetylene carrier gas into the resistively-heated SiC tube without seeding the 4-bromophenanthrene, and also by helium carrier gas with seeding the 4-bromophenanthrene precursor. No signal at *m/z* = 202 was observed in these control experiments.

**Electronic Structure and Rate Constant Calculations**: The calculations of the energies and molecular parameters of various local minima and transition states involved in the reaction were carried out at the G3(MP2,CC)//B3LYP/6-311G(d,p) level of theory.[54-56] This 'model chemistry' theoretical approach is considered to be chemically accurate, as it normally provides accuracy of 0.01–0.02 Å for bond lengths, 1–2° for bond angles, and 3–6 kJ mol$^{-1}$ for relative energies of hydrocarbons and their radicals in terms of average absolute deviations.[46] The GAUSSIAN 09[57] and

MOLPRO 2010[49] program packages were employed for the ab initio calculations. The MESS package[58] was used to solve the one-dimensional master equation and to compute temperature-dependent phenomenological rate constants in the zero- and high pressure limits within the Rice-Rampsberger-Kassel-Marcus Master Equation (RRKM-ME) method. The Rigid-Rotor, Harmonic-Oscillator (RRHO) model was used to compute densities of states and partition functions of local minima and numbers of states of transition states. Low-frequency normal modes were visually examined and those representing internal rotations were considered as one-dimensional hindered rotors in terms of the partition function. B3LYP/6-311G(d,p) calculations were utilized to evaluate one-dimensional torsional potentials for the hindered rotors. Vertical and adiabatic ionization energies of various species were computed at the G3(MP2,CC)//B3LYP/6-311G(d,p) level of theory.

## Data Availability Statement

The data that support the plots within this paper and other findings of this study are available from the corresponding author upon reasonable request.

## Competing financial interests

The authors declare no competing financial interests.

## References Methods

51 Cool, T. A. *et al.* Selective detection of isomers with photoionization mass spectrometry for studies of hydrocarbon flame chemistry. *J. Chem. Phys.* **119,** 8356-8365 (2003).
52 Qi, F. *et al.* Isomeric identification of polycyclic aromatic hydrocarbons formed in combustion with tunable vacuum ultraviolet photoionization. *Rev. Sci. Instrum.* **77,** 084101 (2006).
53 Qi, F. Combustion chemistry probed by synchrotron VUV photoionization mass spectrometry. *Proc. Combust. Inst.* **34,** 33-63 (2013).
54 Curtiss, L. A., Raghavachari, K., Redfern, P. C., Rassolov, V. & Pople, J. A. Gaussian-3 (G3) theory for molecules containing first and second-row atoms. *J. Chem. Phys.* **109,** 7764-7776 (1998).
55 Curtiss, L. A., Raghavachari, K., Redfern, P. C., Baboul, A. G. & Pople, J. A. Gaussian-3 theory using coupled cluster energies. *Chem. Phys. Lett.* **314,** 101-107 (1999).
56 Baboul, A. G., Curtiss, L. A., Redfern, P. C. & Raghavachari, K. Gaussian-3 theory using density functional geometries and zero-point energies. *J. Chem. Phys.* **110,** 7650-7657 (1999).
57 Frisch, M. J. *et al.* Gaussian 09. *Revision A.1 Gaussian Inc., Wallingford CT* (2009).
58 Georgievskii, Y., Miller, J. A., Burke, M. P. & Klippenstein, S. J. Reformulation and solution of the master equation for multiple-well chemical reactions. *J. Phys. Chem. A* **117,** 12146-12154 (2013).

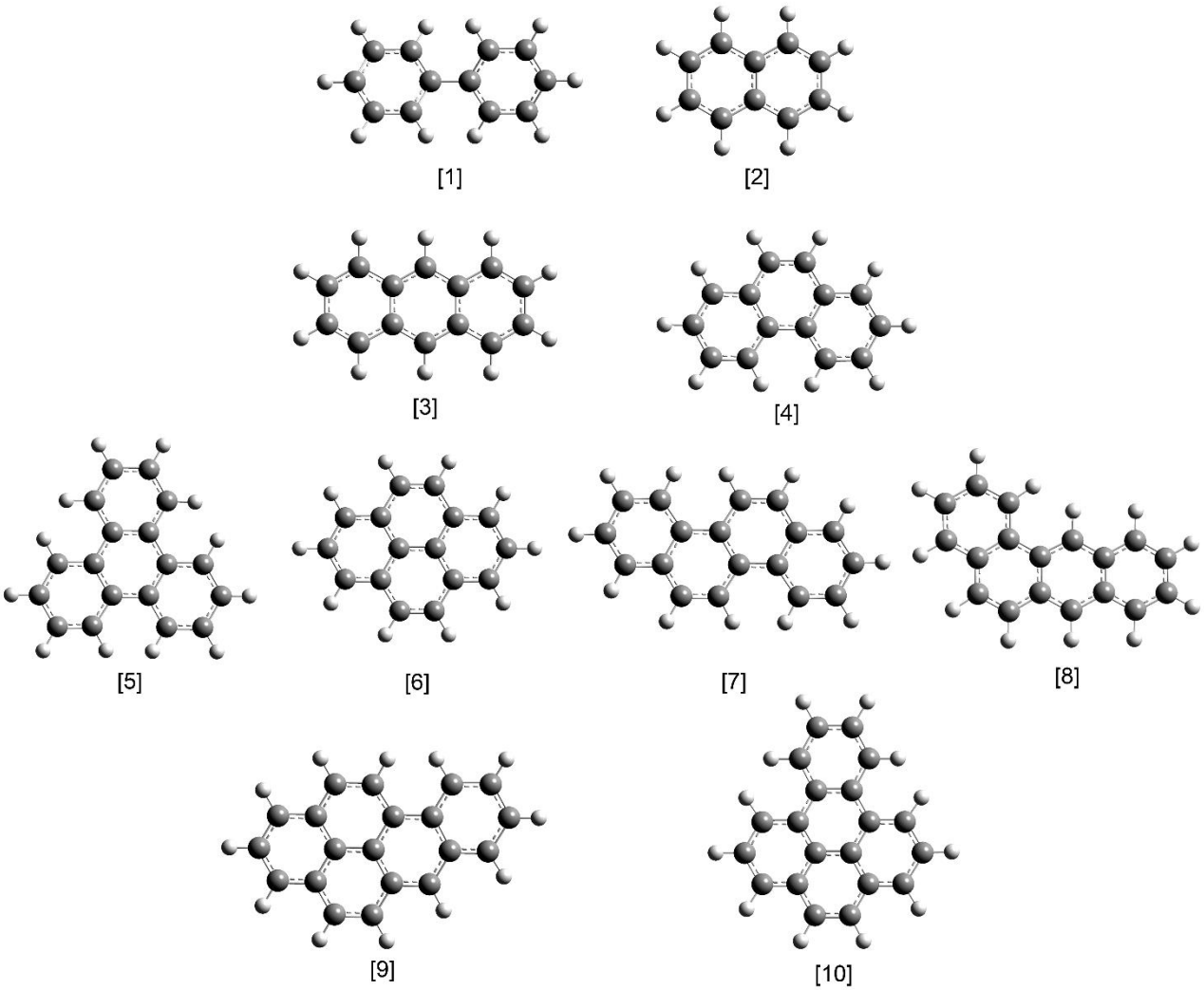


Figure 1

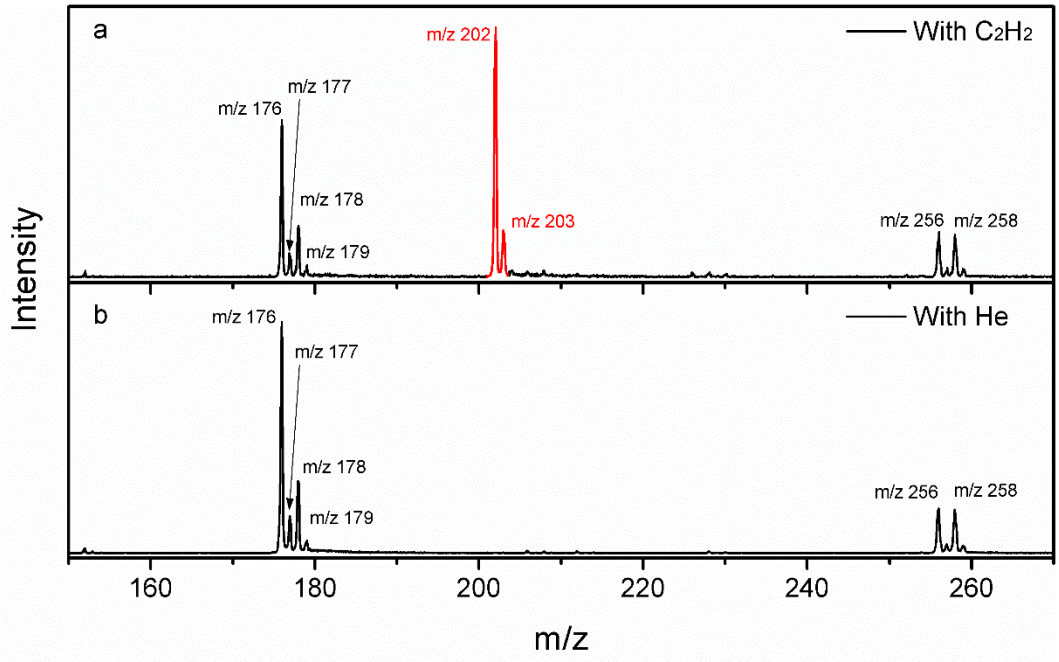
a
With C2H2
m/z 202
m/z 177
m/z 176
m/z 178
m/z 203
m/z 179
m/z 256
m/z 258
b
With He
m/z 176
m/z 177
m/z 178
m/z 179
m/z 256
m/z 258
Intensity
160
180
200
220
240
260
m/z

Figure 2

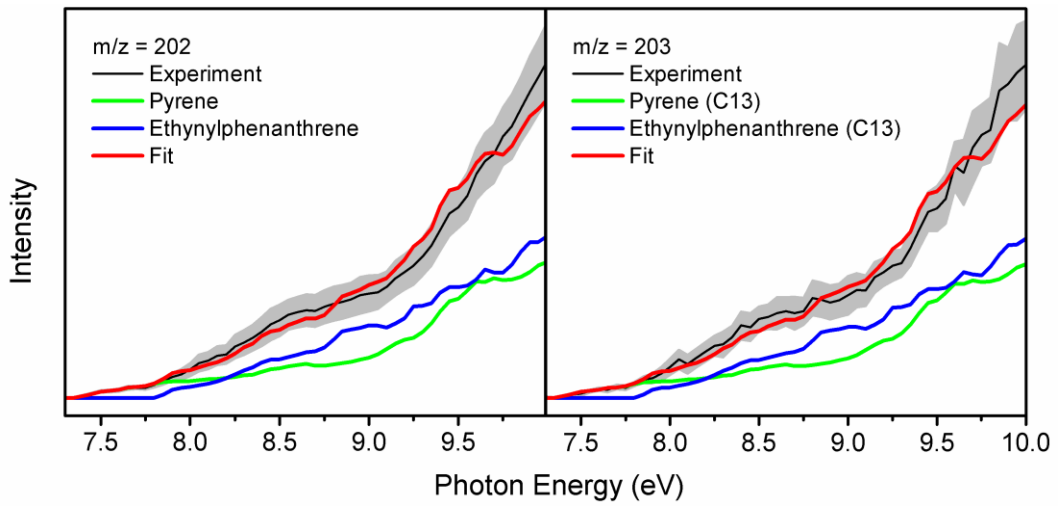
m/z = 202
Experiment
Pyrene
Ethynylphenanthrene
Fit
m/z = 203
Experiment
Pyrene (C13)
Ethynylphenanthrene (C13)
Fit
Intensity
7.5
8.0
8.5
9.0
9.5
7.5
8.0
8.5
9.0
9.5
10.0
Photon Energy (eV)

Figure 3

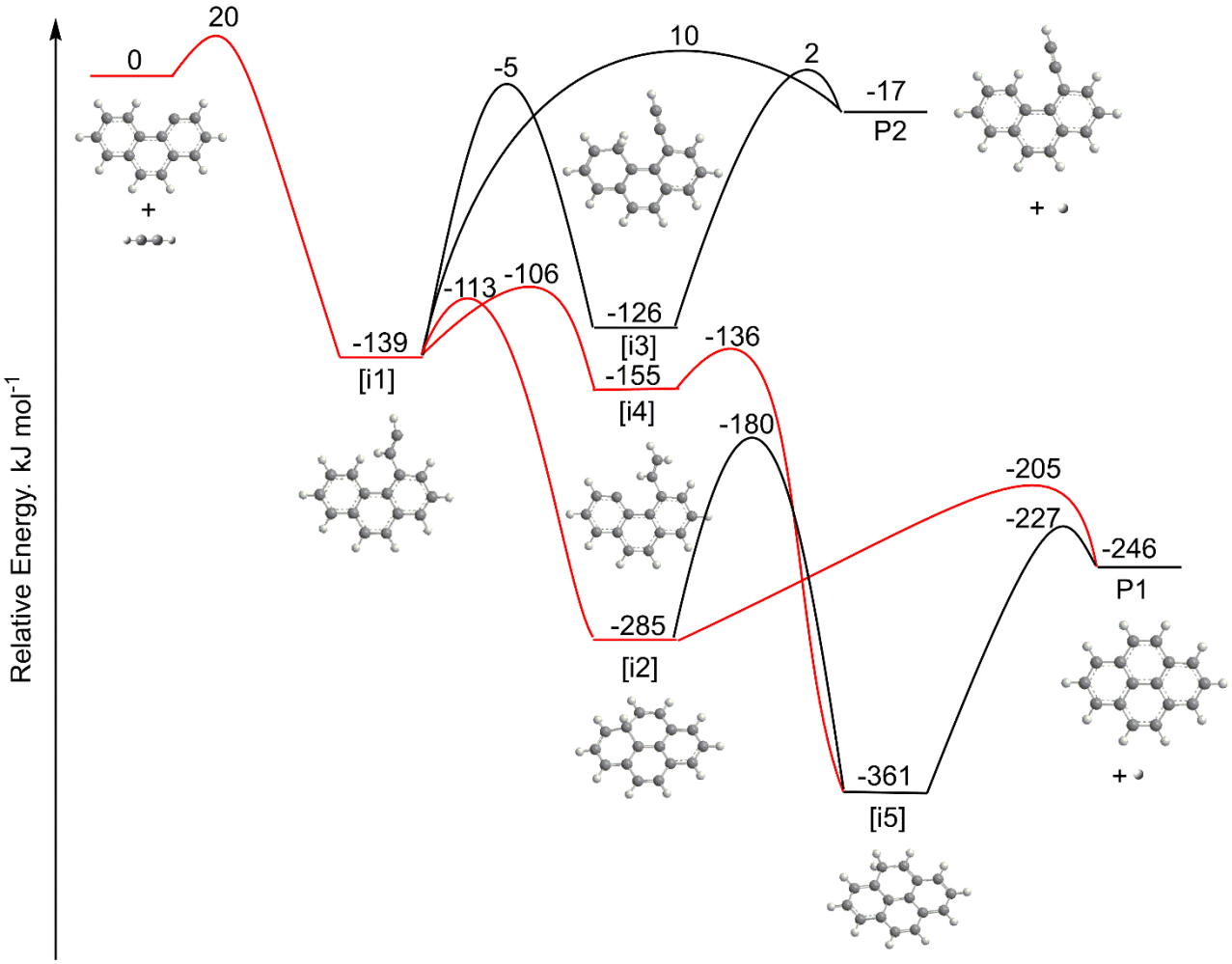
Relative Energy. kJ mol-1
0
20
-139
[i1]
-5
10
2
-17
P2
-113
-106
-126
[i3]
-155
[i4]
-136
-180
-205
-227
-246
P1
-285
[i2]
-361
[i5]
+
+
+

Figure 4

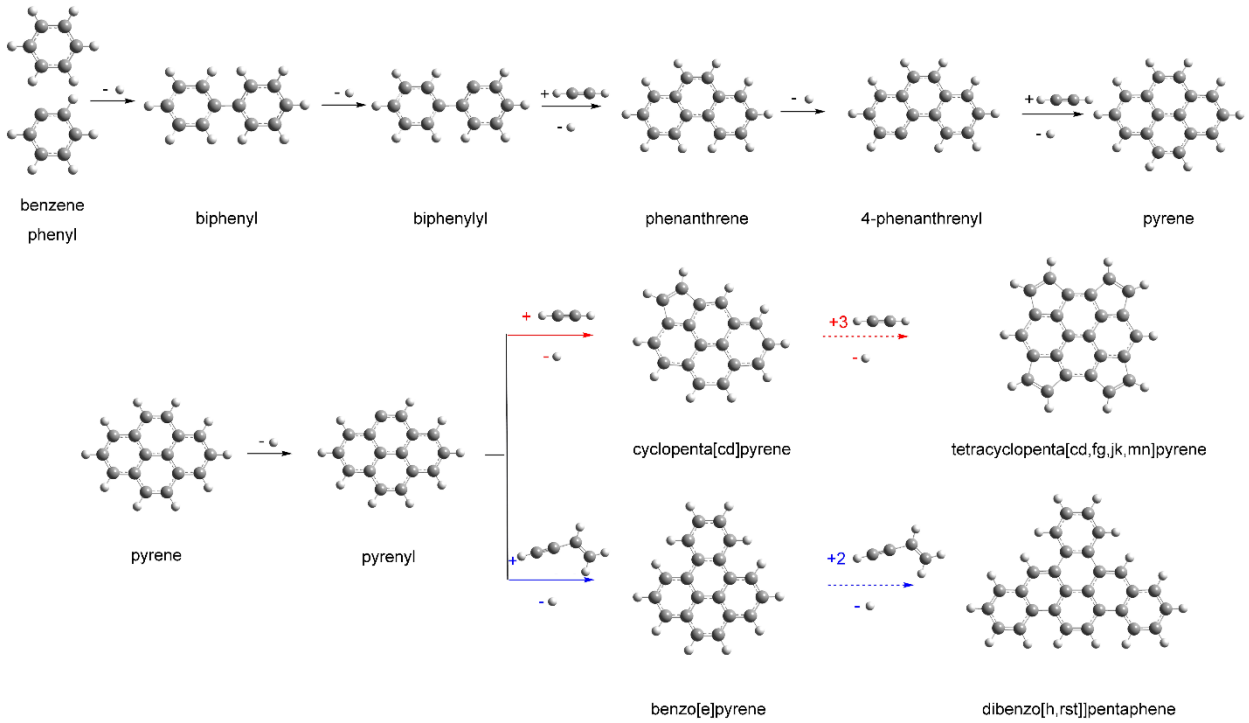
benzene
phenyl
biphenyl
biphenylyl
phenanthrene
4-phenanthrenyl
pyrene
pyrene
pyrenyl
cyclopenta[cd]pyrene
tetracyclopenta[cd,fg,jk,mn]pyrene
benzo[e]pyrene
dibenzo[h,rst]]pentaphene
+3
+2

Figure 5

Supplementary Information

# Pyrene Synthesis in Circumstellar Envelopes and Its Role in the Formation of 2D Nanostructures

**Long Zhao, Ralf. I. Kaiser***

*Department of Chemistry, University of Hawaii at Manoa, Honolulu, HI 96822*

**Bo Xu, Utuq Ablikim, Musahid Ahmed**

*Chemical Sciences Division, Lawrence Berkeley National Laboratory, Berkeley, CA 94720*

**Dharati Joshi, Gregory Veber, Felix R. Fischer**

*Department of Chemistry, University of California, Berkeley, CA 94720, USA*

*Materials Sciences Division, Lawrence Berkeley National Laboratory, Berkeley, CA 94720, USA*

*Kavli Energy NanoSciences Institute at the University of California Berkeley and the Lawrence Berkeley National Laboratory, Berkeley, California 94720, USA*

**Alexander M. Mebel**

*Department of Chemistry and Biochemistry, Florida International University, Miami, FL 33193*

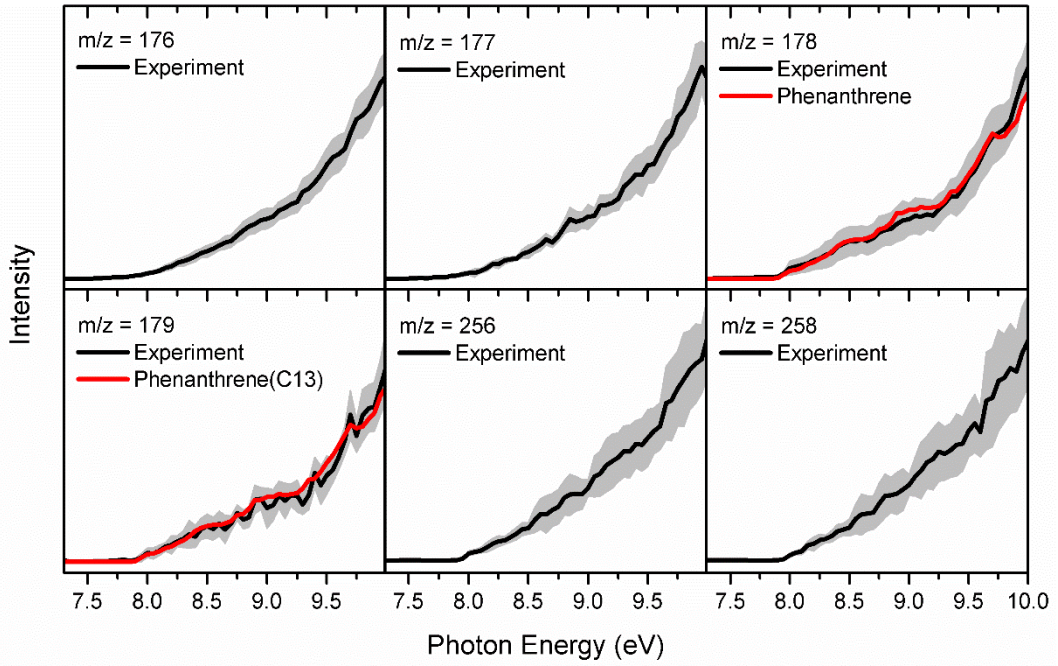


Supplementary Figure 1. PIE curves for additional ions detected in this work. The onset of the ion signal at *m/z* = 176 at 7.90 ± 0.05 eV correlates nicely with the computed adiabatic ionization energies for various phenanthrynes (Figure S2) with computed adiabatic ionization energies of 7.95 ± 0.10, 7.95 ± 0.10, 8.01 ± 0.10, and 8.06 ± 0.10 eV (Table S1). The onset of ion counts at *m/z* = 177 at 7.80 ± 0.05 eV matches the computed adiabatic ionization energy of the 4-phenanthrenyl radical of 7.70 ± 0.10 eV (Table S1). ± 10% uncertainty based on the accuracy of the photodiode and a 1 σ error of the PIE curve averaged over three PIE scans contribute to the overall errors.

Supplementary Table 1. Calculated vertical and adiabatic ionization energies (eV).

| Species | Vertical IE | Adiabatic IE |
|---|---|---|
| 4-phenanthrenyl | 8.56 | 7.70 |
| 4-ethynylphenanthrene | 7.84 | 7.72 |
| 3-ethynylphenanthrene | 7.85 | 7.73 |
| 2-ethynylphenanthrene | 8.00 | 7.84 |
| 1-ethynylphenanthrene | 7.88 | 7.75 |
| 9-ethynylphenanthrene | 7.83 | 7.71 |
| 3,4-phenanthryne | 8.11 | 7.95 |
| 2,3-phenanthryne | 8.10 | 7.95 |
| 1,2-phenanthryne | 8.15 | 8.01 |
| 9,10-phenanthryne | 8.20 | 8.06 |

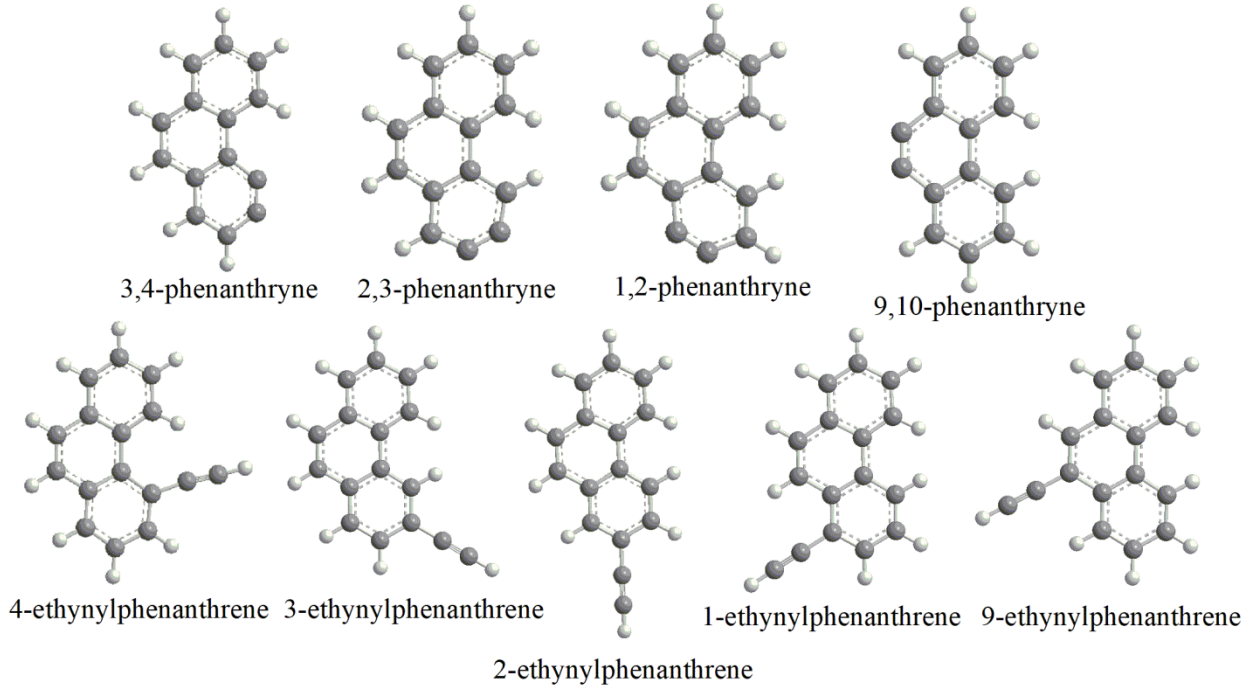


Supplementary Figure 2. Structures of distinct isomers of phenanthrynes and ethynyl-phenanthrenes.

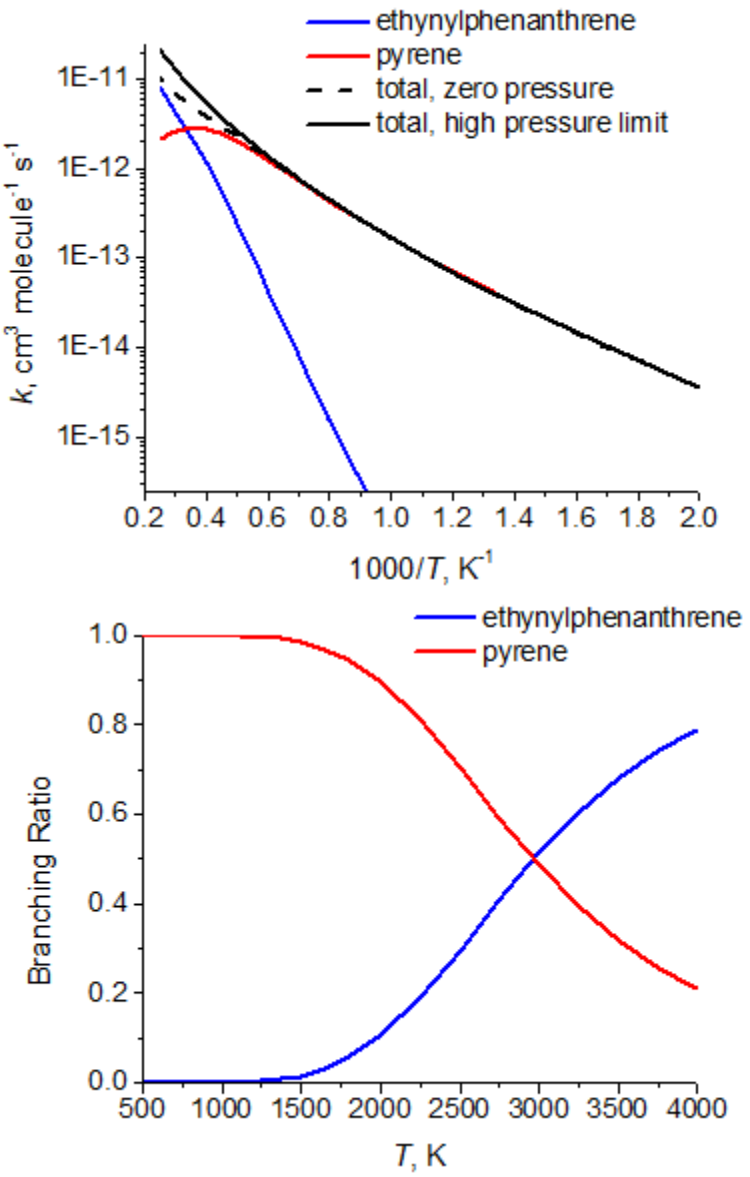


Supplementary Figure 3. Calculated rate constants for the 4-phenanthrenyl + $C_2H_2$ reaction, including the total rate constants and those for the formation of pyrene and 4-ethynylphenanthrene (top) and branching ratios of the two product channels (bottom).

(a)

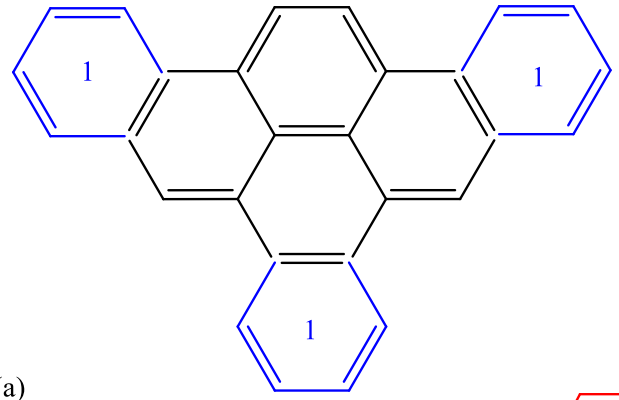


(b)

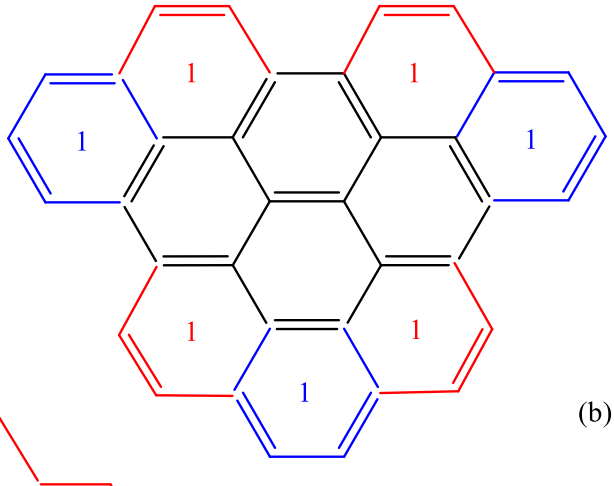


(c)

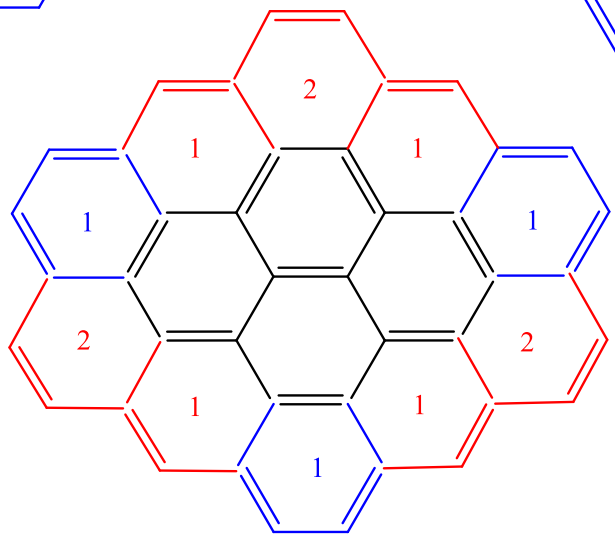


(d)

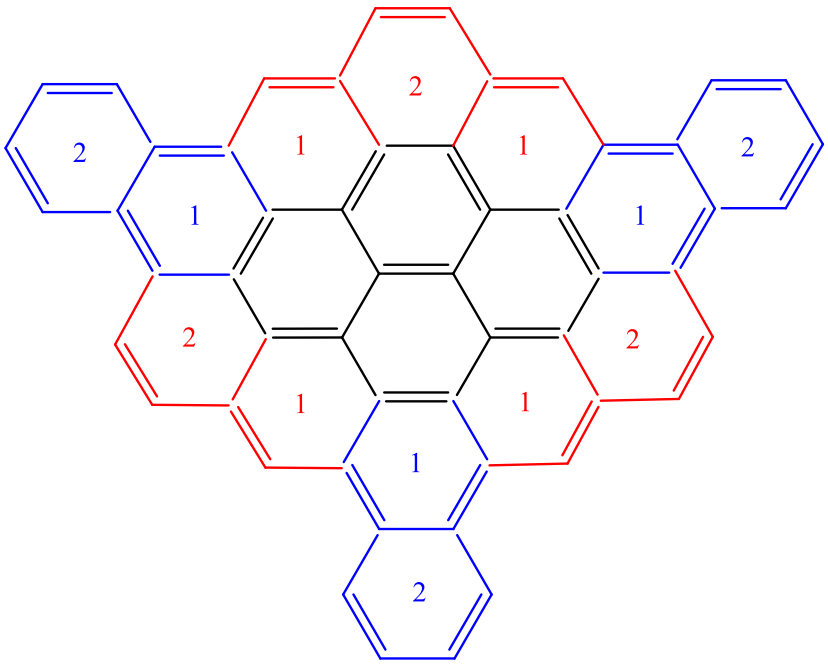

(e)

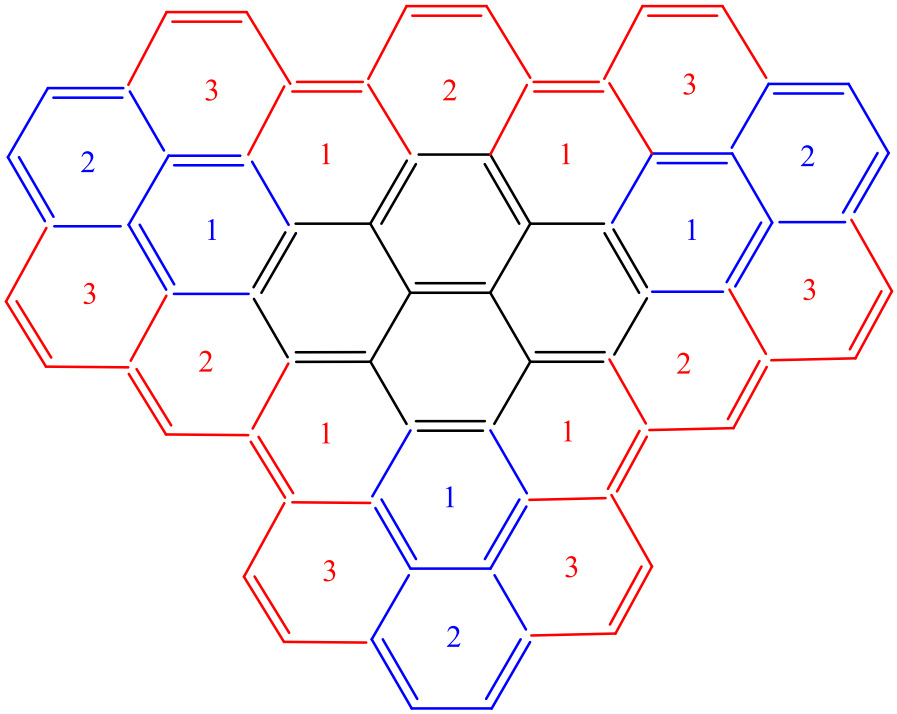


(f)

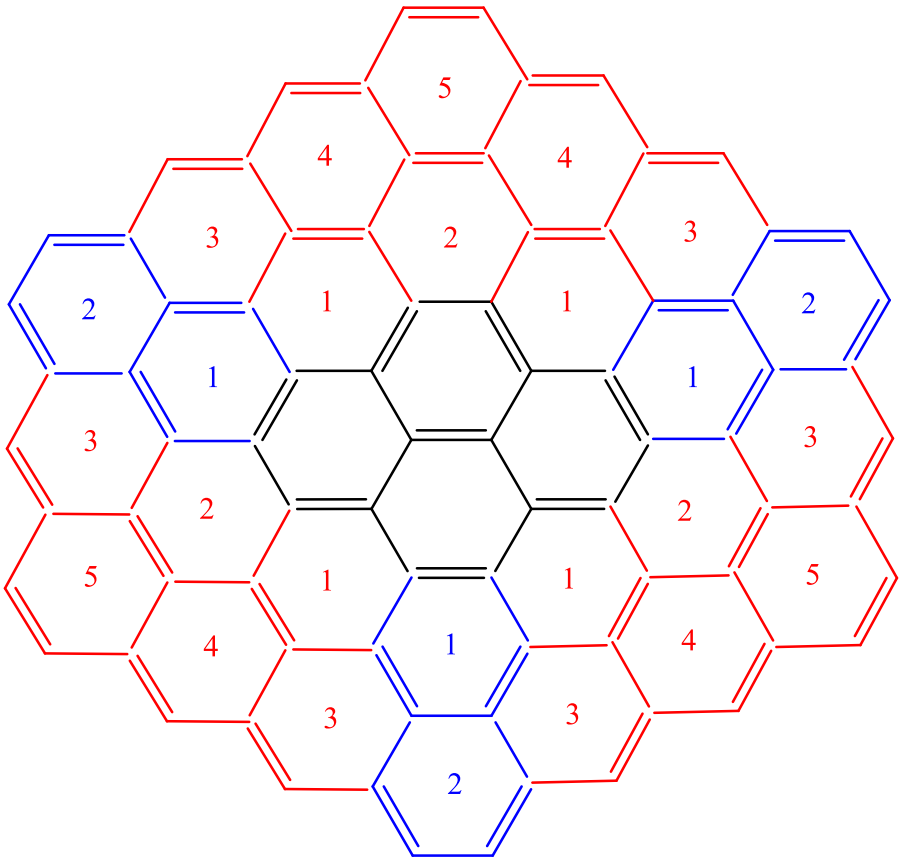

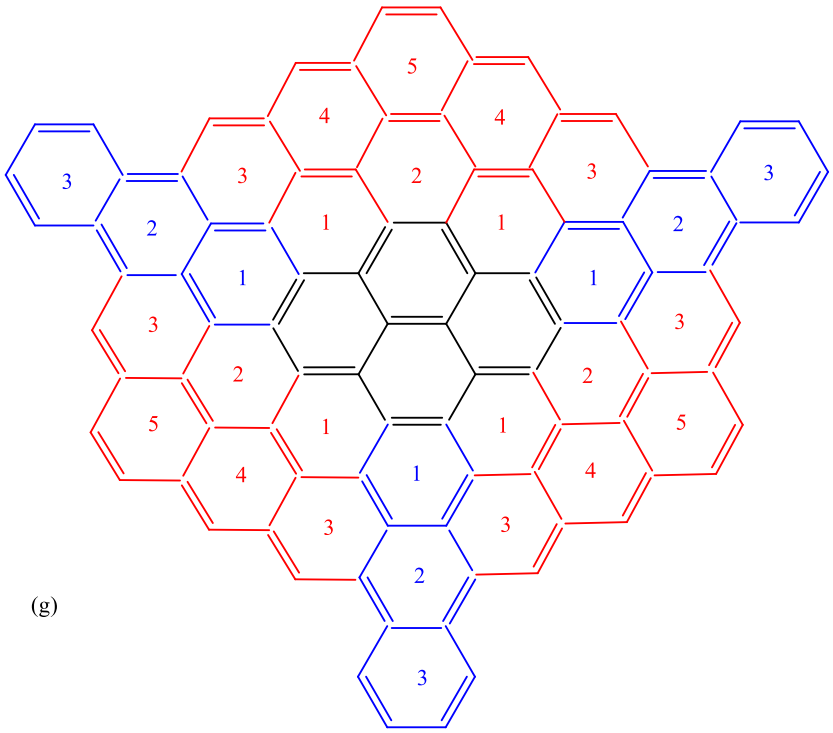
5
4
4
3
3
3
3
2
2
1
1
1
3
2
2
5
1
1
5
4
1
4
3
3
2
3

(g)

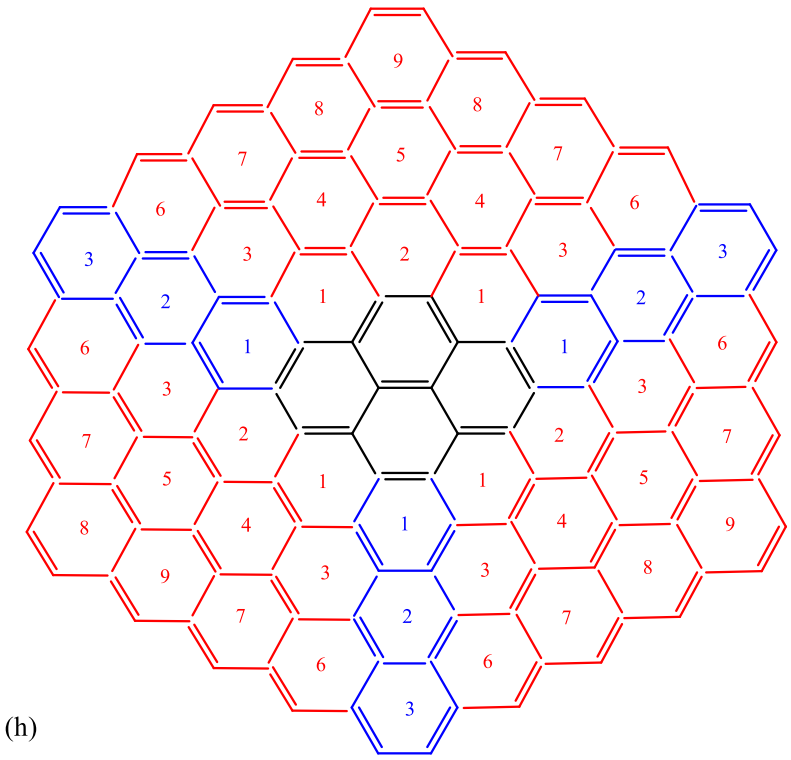
9
8
8
7
5
7
6
4
4
6
3
3
2
3
3
2
1
1
2
6
1
1
6
3
3
7
2
2
7
5
1
1
5
8
4
1
4
9
9
3
3
8
7
2
7
6
6
3

(h)

Supplementary Figure 4. Schematic representation of the central role of the pyrene molecule in the growth of two-dimensional graphene-type nanostructures involving HACA and HAVA pathways. The acetylene and vinylacetylene building blocks for the HACA and HAVA mechanism are color coded in red and blue, respectively. HAVA leads to an acene-type growth in three sectors of the pyrene molecule separated by 120°; HACA accounts for the bay closures. (a) first order perimeter growth (HAVA), (b) first order perimeter growth (HACA), (c) second order perimeter growth (HACA), (d) second order perimeter growth (HAVA), (e) third order perimeter growth (HACA), (f) fourth and fifth order perimeter growth (HACA). Once HACA closes the bays, HAVA initiates a third order perimeter growth (HAVA) (g) to supply new bays to be closed (h). The numbers in red and blue define the order of the HACA and HAVA growth, respectively.

Synthesis of 4-bromophenanthrene

Materials and General Methods. Unless otherwise stated, all manipulations of air and/or moisture sensitive compounds were carried out in oven-dried glassware, under an atmosphere of $N_2$. All solvents and reagents were purchased from Alfa Aesar, Spectrum Chemicals, Acros Organics, TCI America, and Sigma-Aldrich and were used as received unless otherwise noted. Organic solvents were dried by passing through a column of alumina and were degassed by vigorous bubbling of $N_2$ or Ar through the solvent for 20 min. Flash column chromatography was performed on SiliCycle silica gel (particle size 40–63 μm). Thin layer chromatography was carried out using SiliCycle silica gel 60 Å F-254 precoated plates (0.25 mm thick) and visualized by UV absorption. All $^1$H and $^{13}$C NMR spectra were recorded on Bruker AVB-400, AVQ-400, AV-600 MHz spectrometers, and are referenced to residual solvent peaks ($CDCl_3$ $^1$H NMR = 7.26 ppm, $^{13}$C NMR = 77.16 ppm or $CD_2Cl_2$ $^1$H NMR = 5.32 ppm, $^{13}$C NMR = 54.00 ppm). ESI mass spectrometry was performed on a Finnigan LTQFT (Thermo) spectrometer in positive ionization mode.

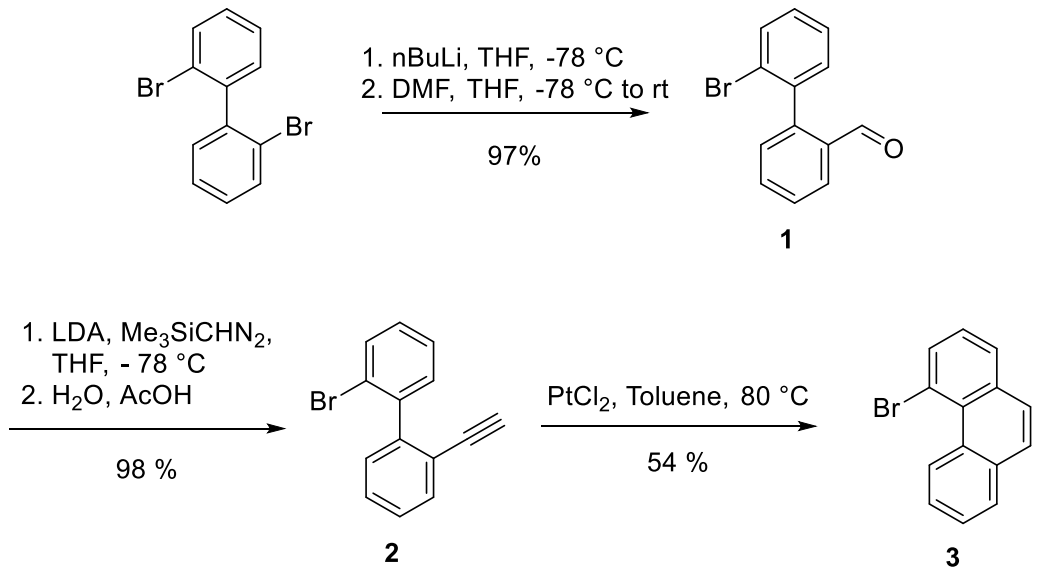


Supplementary Figure 5. Synthesis of 4-bromophenanthrene (3)

**Synthetic procedures.**

*2'-bromo-[1,1'-biphenyl]-2-carbaldehyde* (**1**) (Figure S5) A 250 mL Schlenk flask was charged under $N_2$ with 2,2'-dibromo-1,1'-biphenyl (4.46 g, 14.3 mmol) in dry THF (86 mL). The reaction mixture was cooled to –78 °C. n-BuLi (2.5M in hexanes, 5.7 mL, 14.3 mmol) was added dropwise over 15 min and the reaction mixture was stirred for 15 min at –78 °C. DMF (2.6 mL, 33.7 mmol) in dry THF (13 mL) was then added dropwise. The reaction mixture was warmed to 24 °C and stirred for 18 h. The reaction mixture was quenched with saturated aqueous $NH_4Cl$ (100 mL) and extracted with $CH_2Cl_2$. The combined organic phases were washed with $H_2O$ and saturated aqueous NaCl, dried over $MgSO_4$, and concentrated on a rotary evaporator. Column chromatography ($SiO_2$; 0–2% EtOAc/hexane) yielded **1** (3.64 g, 13.9 mmol, 97%) as a colorless viscous oil that solidified into a colorless solid over time. $^1$H NMR (400 MHz, $CDCl_3$, 22 °C) δ = 9.77 (d, *J* = 0.8 Hz, 1H), 8.00 (dd, *J* = 7.7, 1.5 Hz, 1H), 7.74–7.65 (m, 2H), 7.57 (dddd, *J* = 7.6, 7.6, 1.1, 1.1 Hz, 1H), 7.44 (ddd, *J* = 7.5, 7.5, 1.2 Hz, 1H), 7.38–7.30 (m, 3H) ppm; $^{13}$C {$^1$H} NMR (101 MHz, $CDCl_3$, 22 °C) δ = 191.8, 144.9, 139.5, 134.3, 134.2, 133.2, 132.2, 131.4, 130.3, 129.1, 128.0, 127.8, 124.3 ppm; FTMS (EI+) m/z: $[M–H]^+$ calcd. $[C_{13}H_8OBr]^+$ 259.9660; found 259.9670.

*2-bromo-2'-ethynyl-1,1'-biphenyl* (**2**) (Figure S5) A 100 mL Schlenk flask was charged under $N_2$ with LDA (2 M in THF/n-heptane/ethyl benzene, 8.4 mL, 16.7 mmol) in dry THF (7.2 mL). The reaction mixture was cooled to –78 °C and $Me_3SiCHN_2$ (2 M in diethyl ether, 8.4 mL, 16.7 mmol) was added dropwise. The reaction mixture was stirred at –78 °C for 30 min. **1** (3.64 g, 13.9 mmol) in dry THF (17 mL) was added dropwise and the reaction mixture was stirred at 24 °C for 5 h. The reaction mixture was quenched with $H_2O$ and AcOH until gas evolution stopped, and extracted with $CH_2Cl_2$. The combined organic phases were washed with $H_2O$ and saturated aqueous NaCl, dried over $MgSO_4$, and concentrated on a rotary evaporator. Column chromatography ($SiO_2$; 0–2% $CH_2Cl_2$/hexane) yielded **2** (3.51 g, 13.7 mmol, 98%) as a colurless oil. $^1$H NMR (400 MHz, $CDCl_3$, 22 °C) δ = 7.68 (dd, *J* = 8.0, 1.3 Hz, 1H), 7.62 (dd, *J* = 7.8, 1.4 Hz, 1H), 7.47–7.36 (m, 3H), 7.33 (dd, *J* = 7.6, 1.9 Hz, 1H), 7.30–7.24 (m, 2H), 3.01 (s, 1H) ppm; $^{13}$C {$^1$H} NMR (101 MHz, $CDCl_3$, 22 °C) δ = 144.2, 141.5, 133.0, 132.7, 131.4, 129.9, 129.3, 128.6, 127.8, 127.1, 123.5, 121.8, 82.3, 80.5 ppm; FTMS (EI+) m/z: $[C_{14}H_9Br]^+$ calcd. $[C_{14}H_9Br]^+$ 255.9888; found 255.9889.

*4-bromophenanthrene* (**3**) (Figure S5) A 50 mL Schlenk flask was charged under $N_2$ with **2** (1.16 g, 4.51 mmol) and $PtCl_2$ (120 mg, 0.45 mmol) in dry toluene (22 mL). The reaction mixture was

stirred at 80 °C for 24 h. The reaction was cooled to 24 °C and concentrated on a rotary evaporator. Column chromatography ($SiO_2$; hexanes) yielded **3** (623 mg, 2.42 mmol, 54 %) as a colorless solid. $^1$H NMR (400 MHz, $CDCl_3$, 22 °C) δ = 10.06–10.00 (m, 1H), 8.01 (dd, *J* = 7.6, 1.4 Hz, 1H), 7.95–7.91 (m, 1H), 7.89 (dd, *J* = 7.8, 1.4 Hz, 1H), 7.78 (d, *J* = 8.8 Hz, 1H), 7.71 (d, *J* = 8.8 Hz, 1H), 7.69–7.63 (m, 2H), 7.41 (dd, *J* = 7.7, 7.7 Hz, 1H) ppm; $^{13}$C {$^1$H} NMR (101 MHz, $CD_2Cl_2$, 22 °C) δ = 135.7, 135.3, 134.0, 130.2, 129.5, 129.1, 129.0, 128.7, 127.7, 127.6, 127.3, 127.2, 125.9, 119.9 ppm. The NMR spectra are shown in Figures S6-S11.

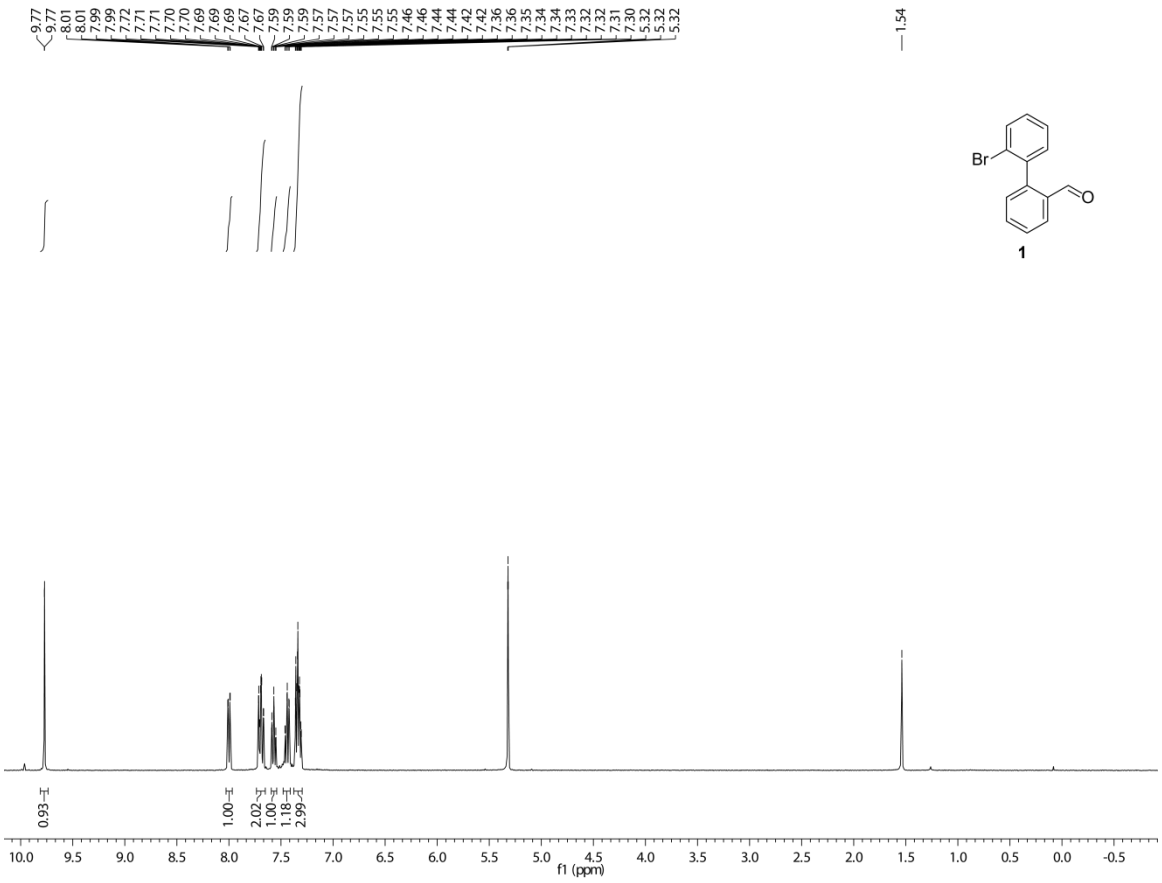


Supplementary Figure 6. $^{1}$H NMR (400 MHz, $CD_2Cl_2$) spectrum of **1**.

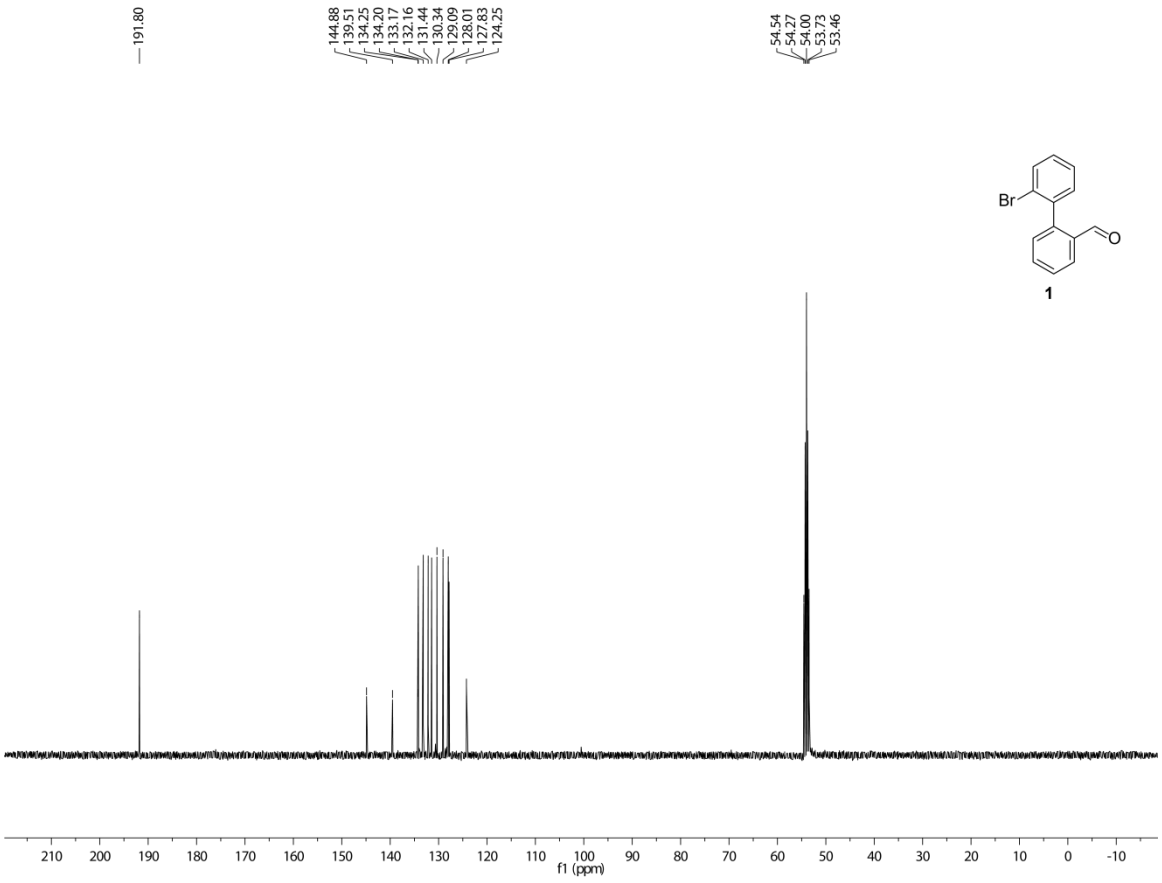


Supplementary Figure 7. $^{13}C$ NMR (101 MHz, $CD_2Cl_2$) spectrum of **1**

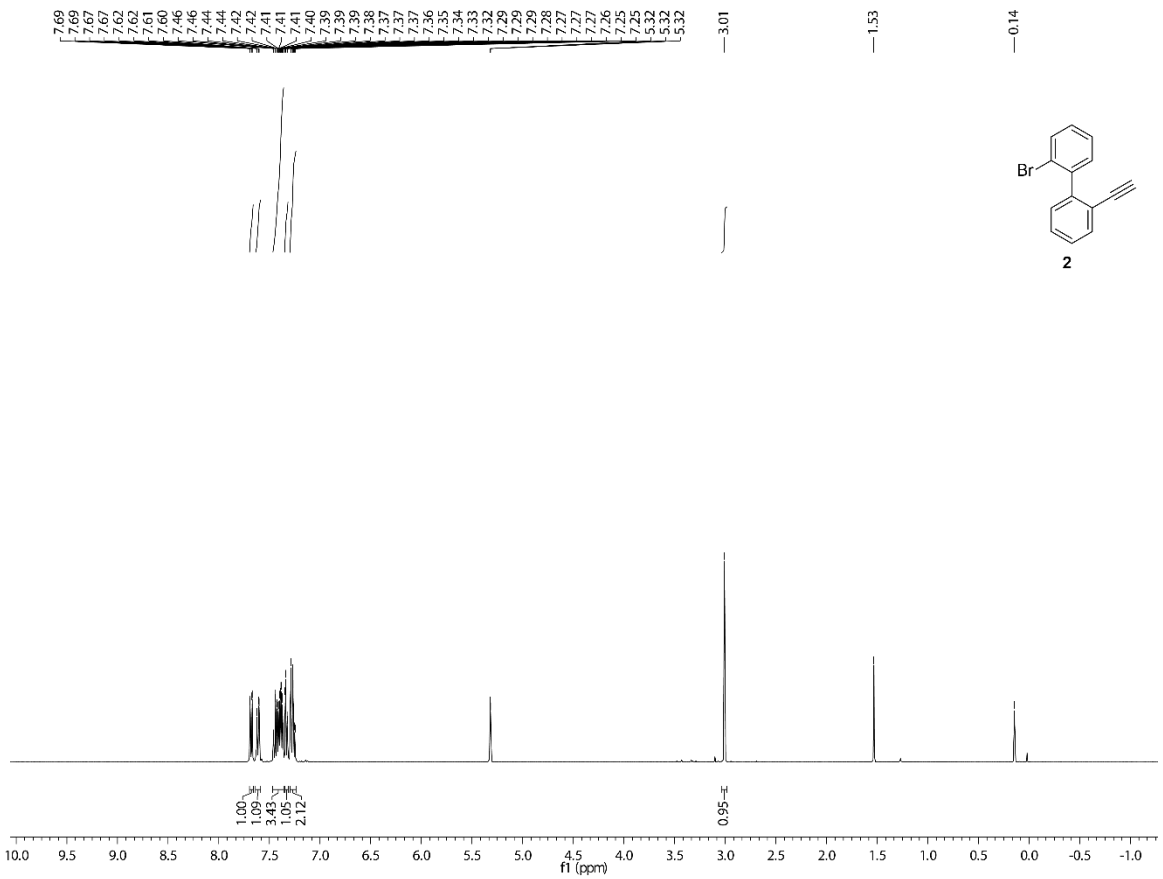


Supplementary Figure 8. $^{1}H$ NMR (400 MHz, $CD_2Cl_2$) spectrum of **2**.

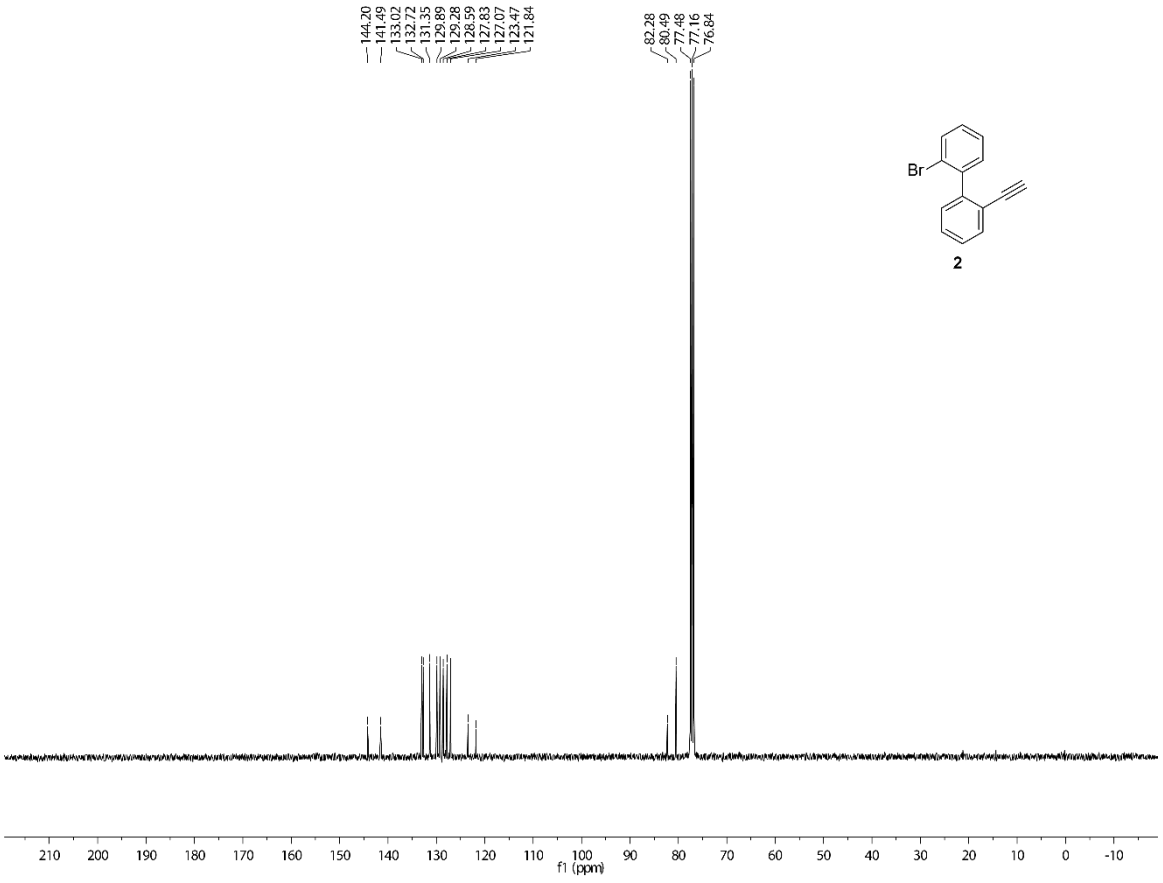


Supplementary Figure 9. $^{13}C$ NMR (101 MHz, $CDCl_3$) spectrum of **2**

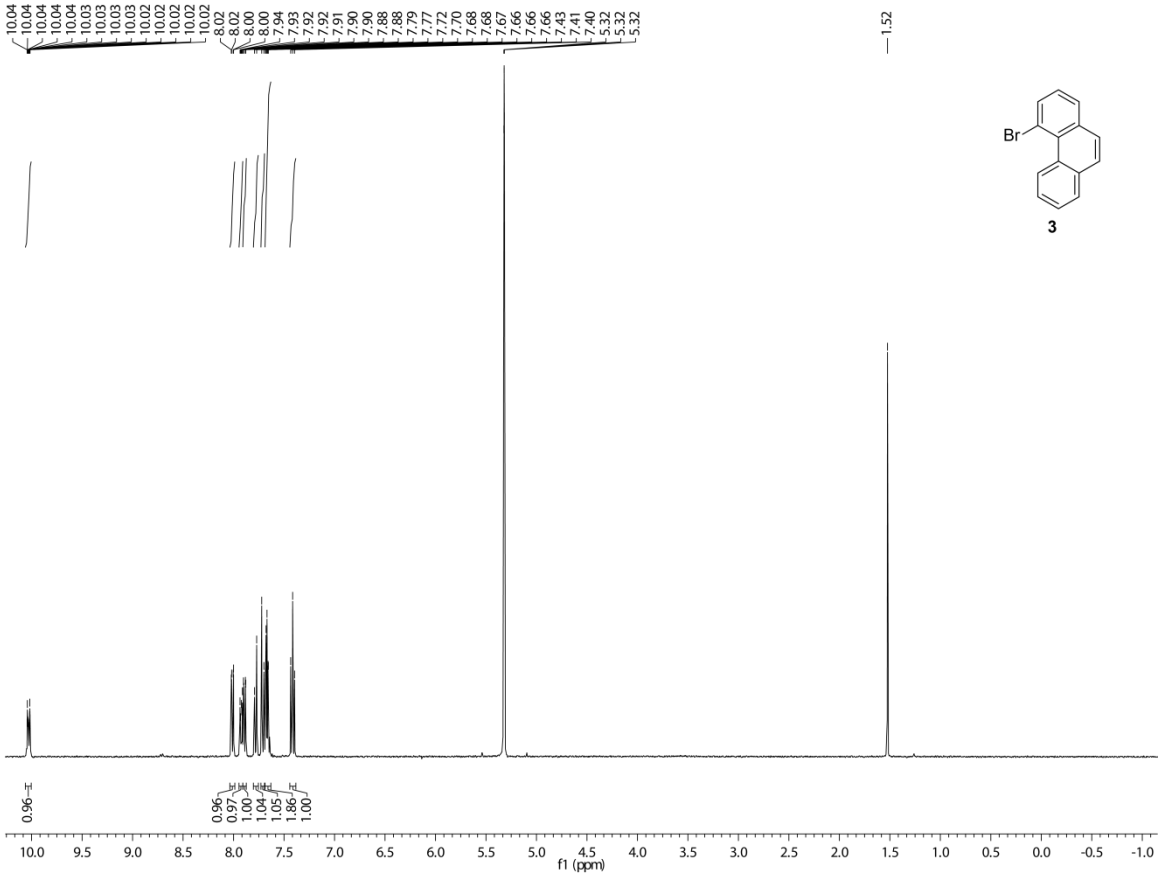


Supplementary Figure 10. $^{1}H$ NMR (400 MHz, $CD_2Cl_2$) spectrum of **3**.

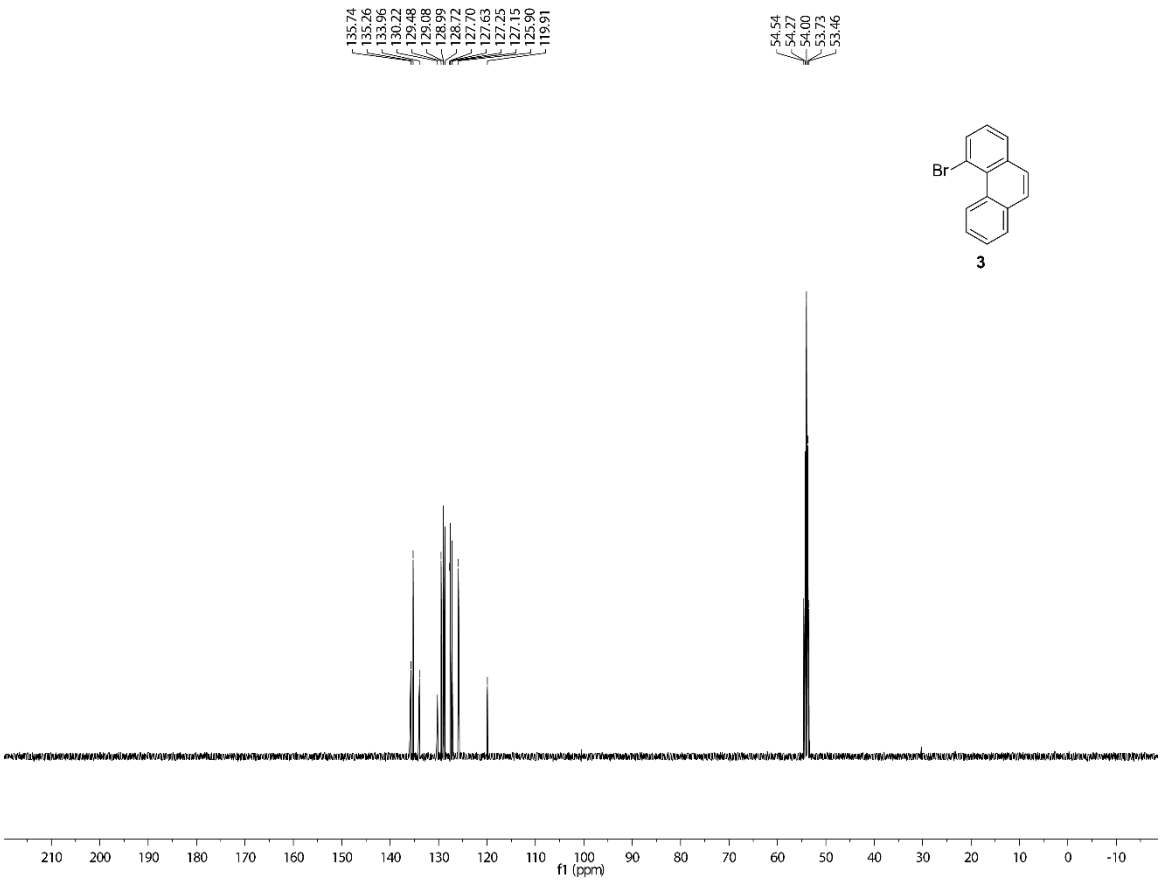


Supplementary Figure 11. $^{13}C$ NMR (101 MHz, $CD_2Cl_2$) spectrum of **3**